Periodic box Fermi hypernetted chain calculations of neutron star crustal matter

Nicola Bassan*
SISSA, I-34136 Trieste, Italy and INFN, Sezione di Trieste, I-34136 Trieste, Italy

Stefano Fantoni†
ANVUR, National Agency for the Evaluation of Universities and Research Institutes, 20 P. za Kennedy, I-00144 Rome, Italy

Kevin E. Schmidt‡
Department of Physics, Arizona State University, Tempe, Arizona 85287, USA
(Received 16 June 2011; published 19 September 2011)

Neutron star crustal matter, whose properties are relevant in many models aimed at explaining observed astrophysical phenomena, has so far always been studied using a mean-field approach. To check the results obtained in this way, a sensible next step is to make use of a realistic nuclear potential. The present paper extends the periodic box Fermi hypernetted chain method to include longitudinal-isospin dependence of the correlations, making feasible a study of asymmetric crustal matter. Results are presented for the symmetry energy, the low-density neutron star equation of state, and the single-particle neutron and proton energies.

DOI: 10.1103/PhysRevC.84.035807 PACS number(s): 26.60.Kp, 26.60.Gj

I. INTRODUCTION

Various observed phenomena connected with neutron stars (NS)—such as glitches—are thought to be largely determined by their crustal properties. Glitches are abrupt changes in pulsar periods,[1] widely thought to be related either to starquakes or to vortex pinning, although there are also other possibilities [2]. A key role in these interruptions in the usually regular behavior of the pulsar spin period is thought to be played by the interaction between superfluid neutrons and normal matter in the crust.

Although a number of recent papers have focused on studying NS crustal properties (e.g., [3,4]), none of them have gone beyond a mean-field approach for describing the nuclear interaction. That sort of approach allows one to give a self-consistent description of all of the nucleons forming the crustal matter, either as part of the large neutronized neutron-drip nuclei which form the lattice or as part of the neutron superfluid which flows through it. (For a recent review of NS crustal matter, see Ref. [2]). However, major advances have been made in recent years in developing nuclear many-body methods for dealing with strongly interacting fermions, which have enabled very accurate calculations to be made of several properties of nucleonic matter at low temperature, in both normal and superfluid phases, which have clearly shown that *NN* correlations play a fundamental role and cannot be disregarded. The short-range behavior of these arises from the strong repulsion of the nuclear potential at short internucleon distances, and the long-range behavior results from the tensor interaction coming from pion exchange. These types of behavior have proved to be a distinctive feature of *NN* correlations and hence of the nuclear medium, and they lead to potentially measurable effects related to NS structure and the neutrino mean free path [5].

These technical advances make it possible to perform *ab initio* calculations of the structural properties of the NS nuclear medium, all the way from the crust to the inner core, fully based on a realistic bare *NN* interaction. This paper is concerned with addressing this challenging problem.

Obviously, *ab initio* calculations have a much more limited range of applications than calculations with mean-field theories which, however, are based on *ad hoc* effective interactions, which are supposed to include the main features of the *NN* correlations in some average way. Therefore, a second important goal of these studies is to derive mean-field effective interactions from first principles, starting from a unique bare nuclear interaction.

We base our investigation here on orthogonal correlated basis theory (OCB) [6–9] and nuclear quantum Monte Carlo (QMC) methods, particularly variational Monte Carlo (VMC) and auxiliary field diffusion Monte Carlo (AFDMC) [10]. All of these methods enable one to make very accurate calculations of nuclear matter interacting with modern *NN* potentials, but they have all only been used so far for homogeneous matter, for nuclei, or for neutron droplets. The NS crustal matter is composed of a lattice of neutron-rich nuclei surrounded by superfluid neutrons. Typical mixtures are characterized by a lattice length of ∼20–60 fm and density values of the neutron soup ranging from $\sim 0.001\,\mathrm{fm}^{-3}$ to $\sim 0.1\,\mathrm{fm}^{-3}$. In spite of having such relatively low densities, the neutrons are still in a regime of strongly correlated fermions, because the neutron-neutron scattering length is large, $a_{nn} \sim -20$ fm and the resulting values of $k_F a_{nn}$ range from ~ -6 to ~ -30.

As far as QMC is concerned, one has to deal with periodic boxes of dimension ∼20–60 fm, with a heavy nucleus at the center and a few thousand neutrons surrounding it. This requires very resource-intensive simulations, which cannot be massively parallel. Because of this, OCB theory will

*bassan@sissa.it
†fantoni@sissa.it; on leave from SISSA, I-34136 Trieste, Italy.
‡kevin.schmidt@asu.edu
[1]For a statistical study of glitches, see Ref. [1].

be used first to get optimal variational wave functions, and variational estimates of the binding energy per particle (as a function of the neutron density and of the symmetry parameter $\alpha = (N - Z)/A$, as well as for computing quantities like energy spectra, response functions, spectral functions, etc., which are at present beyond the reach of QMC simulations.

In pursuing these goals, we are faced with two kinds of problems: (i) the lattice structure of the NS matter does not allow for calculations in the thermodynamic limit—systems with 2000–3000 neutrons are still far away from that; (ii) we are dealing with asymmetric matter having $N > Z$ and we cannot just rely on using the two extreme cases $\alpha = 0$ and $\alpha = 1$ and then making a quadratic interpolation between them for all of the other cases, because of the presence of the nucleus in the box.

The first of these problems requires relying on the existing periodic box version of the Fermi hyperNetted chain theory (PB-FHNC). The second one requires us to rewrite the PB-FHNC to allow an isospin dependence.

The present paper is devoted to clarifying these two points, which represent fundamental methodological steps toward making a truly microscopic and unified treatment of NS crustal matter. For doing this, we have extended the PB-FHNC method to deal with homogeneous asymmetric nuclear matter described by correlated basis functions, in which the correlation operators have a longitudinal isospin dependence. Further considerations limit the variational choice of the isospin dependence of the correlation operator $\tilde{F}$ to its longitudinal component $\tau_z(i)\tau_z(j)$ only. It is then important to ascertain how good such a variational choice is compared with the full one given by $\tau(i) \cdot \tau(j)$. As a first application, we have considered simple two-body nuclear potentials of the v_4 type, which do not include tensor components but have full spin-isospin dependence. Calculations have been made of the equation of state (EOS) and of the single-particle spectra at various values of symmetry parameter.

The results obtained are very encouraging. The iterative process developed for solving the new PB-FHNC equations converges rapidly and gives stable solutions. Moreover, the longitudinal isospin dependence is able to account for more than 80% of the full isospin dependence for the interaction models which we have considered, irrespective of the values of the density ρ and the symmetry parameter α. Interesting results are obtained for the symmetry energy, particularly in the low-density region. We compare these results with the Bethe-Brueckner-Goldstone (BBG) calculations of Ref. [11].

Since we want to address this paper and subsequent related ones to the astrophysical community, we repeat here some material that was already published in the nuclear physics literature to make the presentation comprehensible. We recognize that readers who are not specialists in nuclear physics will need to be strongly motivated to work through all of this, but we are aiming here to provide a "bridge" for those strongly motivated readers.

The paper is organized as follows. In the next sections we will discuss the nuclear interaction, focusing on the two particular interactions that have been used in our calculations. Then, in Sec. III, we describe the state-dependent particle box FHNC scheme used in this work, and finally we present our results and give conclusions.

II. NUCLEAR POTENTIAL

A realistic nuclear potential is usually written as a two-body potential (e.g., Argonne V18 [12]) plus a three-body contribution (e.g., Urbana IX [13]) which becomes increasingly important beyond half of the nuclear saturation density ($\rho_0 = 0.16\,\mathrm{fm}^{-3} = 2.7 \times 10^{14}\,\mathrm{g\,cm}^{-3}$) (see Ref. [14] and references therein). It was shown that n-body potentials in medium with $n > 2$, can be successfully simulated by two-body density-dependent terms [14,15].

In this paper, we consider the Illinois class of two-body potentials, which are characterized by having a strong local contribution, given by their first six spin-isospin-dependent components:

$$\hat{v}_6(i, j) = \sum_{p=1}^{6} v^{(p)}(r_{ij})\hat{O}_{ij}^{(p)}(i, j), \tag{1}$$

with

$$\hat{O}_{ij}^{p=1-6} = (1, \sigma_{ij}, S_{ij}) \otimes (1, \tau_{ij}), \tag{2}$$

where $\tau_{ij} = \tau_i \cdot \tau_j$ and $\sigma_{ij} = \sigma_i \cdot \sigma_j$, with τ and σ being the Pauli matrices acting, respectively, on the isospin and the spin of a nucleon, and $S_{ij} = (3\hat{r}_{ij}^{\alpha}\hat{r}_{ij}^{\beta} - \delta_{\alpha\beta})\sigma_i^{\alpha}\sigma_j^{\beta}$ is the tensor operator.

The most important nonlocal components of the Illinois potentials are the spin-orbit terms, $\mathbf{L}_{ij} \cdot \mathbf{S}_{ij}$ and $\mathbf{L}_{ij} \cdot \mathbf{S}_{ij}\tau_{ij}$, where $\mathbf{L}_{ij}$ and $\mathbf{S}_{ij}$ are the relative angular momentum and the total spin of the nucleon pair. Model potentials that include the spin-orbit components are denoted as v_8. Other components include L^2, $(\mathbf{L}_{ij} \cdot \mathbf{S}_{ij})^2$ and symmetry breaking operators, giving the total of 18 components of Argonne v_{18} (AV18).

In its full form, AV18 gives an almost perfect fit to the *NN* data up to the meson production threshold. Other realistic *NN* potentials, such as the Bonn and Nijmegen potentials, fit the *NN* data equally well. All of these realistic interactions are more or less equivalent in describing the properties of light nuclei but the latter ones are basically nonlocal, and so they are much more difficult to handle with many-body theories such as OCB and AFDMC. Moreover, *NN* correlations are much better described in r space, in which they are clearly distinguished from relativistic effects.

There is strong evidence that the first eight components of the Illinois-type potentials are sufficient for giving a realistic description of the nuclear medium. Such model potentials can be obtained by simply truncating AV18 after the first eight components. A better choice, however, is to keep the v_8 form and refit the *NN* data. That was done [16], and the corresponding model interaction is known in the literature as Argonne $v_{8'}$ or AV8′. The differences between AV18 and AV8′ are quite small and can safely be treated perturbatively.

Other widely used interaction models from the same class of potentials are $v_{6'}$, which have the form of Eq. (1), and $v_{4'}$, in which the tensor components are also omitted. The AV6′ and AV4′ potentials can be found in Ref. [17]. They should really be

considered only as toy potentials, although they can reproduce a certain amount of nuclear physics data. They are certainly very useful, though, for checking many-body techniques and for finding the relative importance of the tensor and spin-orbit correlations.

One of the potentials which we have used in our calculations is the S3 potential derived by Afnan and Tang by fitting low-energy nucleon-nucleon s-wave scattering data (up to 60 MeV) [18]. This is a v_4 potential of the Serber type, and is therefore defined for only the even states. It provides a reasonable description of some basic properties of H^3 and He^4 such as, for instance, the binding energy and the root-mean-square radii. As in the PB-FHNC calculations of Ref. [19], we have added to the original S3, an interaction for the odd channels given by the repulsive part of the even channels. The four components of the resulting potential, which we denote as the AT4′ potential, are given by

$$\begin{aligned} v^{(1)} &\equiv v_c = v_R + \tfrac{3}{16}(v_{At}(r_{ij}) + v_{As}(r_{ij})), \\ v^{(2)} &\equiv v_\tau = -\tfrac{1}{16}(3v_{At}(r_{ij}) - v_{As}(r_{ij})), \\ v^{(3)} &\equiv v_\sigma = \tfrac{1}{16}(v_{At}(r_{ij}) - 3v_{As}(r_{ij})), \\ v^{(4)} &\equiv v_{\sigma\tau} = -\tfrac{1}{16}(v_{At}(r_{ij}) + v_{As}(r_{ij})), \end{aligned} \tag{3}$$

with the repulsive and attractive components given by

$$\begin{aligned} v_R &= v_{s1}\exp(-\beta_{s1}r^2), \\ v_{As} &= \sum_{i=2}^{3} v_{si}\exp(-\beta_{si}r^2), \\ v_{At} &= \sum_{i=2}^{3} v_{ti}\exp(-\beta_{ti}r^2), \end{aligned} \tag{4}$$

where the strengths v_{si} and v_{ti} and the Gaussian coefficients β_{si} and β_{ti} are given in Ref. [18]. The four components of the AT4′ potentials are compared in Fig. 1.

The PB-FHNC calculations of Ref. [19] were performed for the case of Jastrow correlated theory. The resulting variational energy for a system of 2060 nucleons at the experimental equilibrium density ρ_0 is -15.150 MeV, which is not too far away from the FHNC/SOC result, $E = -16.184$ MeV.

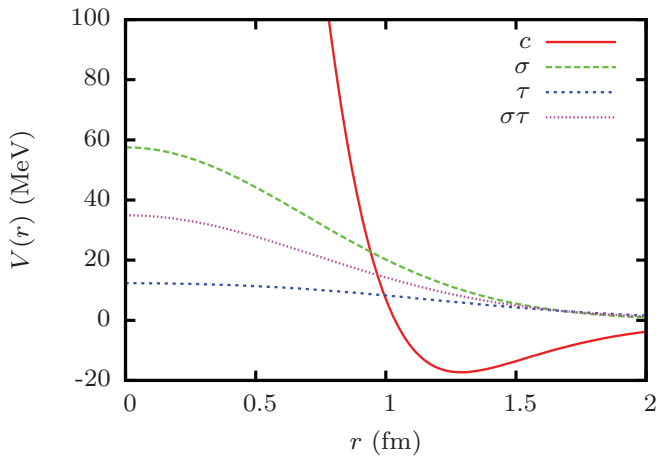

FIG. 1. (Color online) AT4′ potential components.

To compare with the Jastrow results of Ref. [19], we have also performed variational calculations with the potential v_4, obtained by truncating $AV8'$ after its first four components, and denoted here as $(AV8')_4$.

III. CORRELATED BASIS FUNCTIONS

The correlated basis functions for a strongly correlated Fermi fluid are given by

$$|n) = \frac{\hat{F}\,|n]}{[n\,|\,\hat{F}^\dagger\hat{F}\,|n]^{\frac{1}{2}}}, \tag{5}$$

where $|n]$ is a generic eigenfunction of the Fermi gas Hamiltonian and $\hat{F}$ is a correlation operator. The label n indicates the number of particle-hole excitations and $|0]$ denotes the Fermi gas ground state. The set of Fermi gas states $|n]$ is orthonormal, whereas that of the correlated states $|n)$ is not, because the correlation operator $\hat{F}$ breaks the orthogonality. We need to restore orthogonality by following the two-step procedure outlined in Ref. [9]: Orthonormal correlated states are denoted as $|n\rangle$.

A. Properties of the orthonormalization process

It can be shown that the orthonormalization procedure has a number of important properties. Formally in OCB theory, the Hamiltonian H is written as the sum of an unperturbed term H_0 and an interaction term H_I:

$$\begin{aligned} \langle n\,|\,H_0\,|\,m\rangle &= \langle n\,|\,H\,|\,m\rangle\delta_{nm} = H_{nn}\delta_{nm}, \\ \langle n\,|\,H_I\,|\,m\rangle &= \langle n\,|\,H\,|\,m\rangle(1-\delta_{nm}) = \tilde{H}_{nm}. \end{aligned} \tag{6}$$

The interaction Hamiltonian H_I is simply the nondiagonal part of H. The main property of the orthogonalization process of OCB theory is that the diagonal matrix elements are not modified by it, that is,

$$H_{nn} = \langle n\,|\,H\,|\,n\rangle = (n\,|\,H\,|\,n) + \text{terms of order } 1/\Omega. \tag{7}$$

This guarantees that the variational estimates $(I_n\,|\,H\,|\,I_n)$ are maintained after orthogonalization. A second important property is expressed by the following equation:

$$\begin{aligned} (n|H|n) = (0|H|0) &+ \sum_{\mathbf{p}_i} e_v(\mathbf{p}_i) - \sum_{\mathbf{h}_i} e_v(\mathbf{h}_i) \\ &+ \text{terms of order } 1/\Omega. \end{aligned} \tag{8}$$

In this paper we restrict attention to the diagonal matrix elements of the Hamiltonian on the ground state $|0)$ and on the one particle - one hole states $|\mathbf{ph})$, given by

$$(\mathbf{ph}|H|\mathbf{ph}) = \frac{\int dR\mathcal{A}[\phi_1\cdots\phi_A]\hat{F}^\dagger_{JL}H\hat{F}_{JL}\mathcal{A}[\phi_A\cdots\phi_1]}{\int dR\mathcal{A}[\phi_1\cdots\phi_A]\hat{F}^\dagger_{JL}\hat{F}_{JL}\mathcal{A}[\phi_A\cdots\phi_1]}, \tag{9}$$

where $\phi_n = \exp(i\mathbf{k_n}\cdot\mathbf{r_i})\chi_n(s_i)I_n(\tau_i)$ and the orbitals $\phi_1\cdots\phi_A$ correspond to the Fermi sea states in the case of the ground-state energy ($\mathbf{p} = \mathbf{h} = \mathbf{k}_F$) and include the excited state orbital $\mathbf{p}$ in place of the Fermi sea state orbital $\mathbf{h}$ in the case of the particle-hole excitation. $\mathcal{A}$ is the antisymmetrization operator.

Therefore $\mathcal{A}[\phi_1 \dots \phi_A]$ is a Slater determinant of plane waves. Note that in a periodic box treatment, one has a finite number of nucleons and a fixed value for the length $L = \Omega^{1/3}$ of the box, given by $\rho_p + \rho_n = \rho = A/\Omega$.

Integration over dR extends to all of the a coordinates ($R \equiv \mathbf{r}_1, \mathbf{r}_2, \dots, \mathbf{r}_A$) and includes summation over all of the spin and isospin variables.

B. The correlation operator

Since we are considering a v_4 model interaction, we do not need to include tensor correlations in $\hat{F}$. In this case, the standard choice is given by

$$\hat{F}_4 = \mathcal{S}\left\{\prod_{i<j=1}^{A} \hat{f}_4(i,j)\right\} = \mathcal{S}\left\{\prod_{i<j=1}^{A}\left[\sum_{p=1}^{4} f^{(p)}(\mathbf{r}_{ij})\hat{O}_{ij}^{(p)}(i,j)\right]\right\}, \quad (10)$$

where the symmetrization is needed because, in general, the operators $\hat{O}_{ij}^{(p)}$ do not commute with each other. In the calculation of the matrix elements of any given operator, it is not known how all of the orderings of the right-hand side of Eq. (10) can be taken into account. The best known approximation is the so-called FHNC/SOC [20], which was shown to give reliable results in a number of nuclear matter calculations. However, this approximation cannot be used for asymmetric nuclear matter because of the presence of the operator $\tau(i)\cdot\tau(j)$ in $\hat{F}_4$. Because of this, it is important to check the variational relevance of the longitudinal isospin-dependent operator $\hat{O}_{\tau_z}(i,j) = \tau_z(i)\tau_z(j)$ as compared with $\tau(i)\cdot\tau(j)$. The operators $\hat{O}_{\tau_z}(i,j)$ commute with each other, and so can easily be used in asymmetric nuclear matter calculations. To achieve this goal, we consider the following correlation operator:

$$\hat{F}_{JL} = \prod_{i<j=1} [f_{NN}(\mathbf{r}_{ij})P_{NN}(i,j) + f_{PP}(\mathbf{r}_{ij})P_{PP}(i,j) + f_{NP}(\mathbf{r}_{ij})P_{NP}(i,j) + f_{PN}(\mathbf{r}_{ij})P_{PN}(i,j)], \quad (11)$$

where the projection operators P_{ab} are given by

$$\begin{aligned} P_{NN}(i,j) &= \frac{1+\tau_z(i)}{2}\frac{1+\tau_z(j)}{2}, \\ P_{PP}(i,j) &= \frac{1-\tau_z(i)}{2}\frac{1-\tau_z(j)}{2}, \\ P_{NP}(i,j) &= \frac{1+\tau_z(i)}{2}\frac{1-\tau_z(j)}{2}, \\ P_{PN}(i,j) &= \frac{1-\tau_z(i)}{2}\frac{1+\tau_z(j)}{2}. \end{aligned} \quad (12)$$

The four scalar functions f_{NN}, f_{PP}, f_{NP}, and f_{PN} have to heal smoothly to 1, thus giving an uncorrelated system, for r_{ij} greater than a certain *healing distance* d chosen so as to minimize the ground-state energy per particle of the system $(0|H|0)/A$. The results discussed in this paper are obtained under the following assumption:

$$\begin{aligned} f_{NN}(\mathbf{r}_{ij}) &= f_{PP}(\mathbf{r}_{ij}) = f_{\parallel}(\mathbf{r}_{ij}), \\ f_{NP}(\mathbf{r}_{ij}) &= f_{PN}(\mathbf{r}_{ij}) = f_{\perp}(\mathbf{r}_{ij}). \end{aligned} \quad (13)$$

The correlation functions $f_{\parallel}(\mathbf{r}_{ij})$ and $f_{\perp}(\mathbf{r}_{ij})$ are obtained by solving a set of second-order differential equations [20] whose detailed application to the system at hand is described in Appendix A. They distinguish isospin parallel from isospin antiparallel correlations. Such isospin dependence does not completely resolve the difference between $T = 1$ and $T = 0$ channels as in the case of $\hat{F}_4$ of Eq. (10). Nevertheless, as will be shown in this paper, it still provides a very good description of the isospin dependence of nuclear correlations induced by a nuclear two-body potential of the v_4 type.

IV. POWER SERIES EXPANSION AND DIAGRAMMATIC RULES

The CBF matrix elements given in Eq. (9) are calculated by first applying standard Fantoni–Rosati (FR) cluster expansion techniques [21,22] to $(\mathbf{ph}|H|\mathbf{ph})$ and by summing up the resulting series of cluster terms using the FHNC integral equation methods. The FR expansion is based on expanding both the numerator and the denominator of Eq. (9) in powers of the functions $h_\alpha(r)$ given by

$$h_\alpha(\mathbf{r}) = f_\alpha^2(\mathbf{r}) - 1\,, \quad (\alpha = NN, PP, NP, PN). \quad (14)$$

The quantity $\hat{F}_{JL}^\dagger \hat{F}_{JL}$ appearing in the denominator of Eq. (9) is then decomposed into a series of cluster operators as follows:

$$\hat{F}_{JL}^\dagger \hat{F}_{JL} = \frac{A(A-1)}{2}\hat{f}^2(1,2)\left[1 + \sum_{i\neq 1,2}^{A} \mathcal{X}^{(3)}(1,2;i) + \cdots\right], \quad \hat{f}^2(1,2) = \sum f_\alpha^2(\mathbf{r}_{12})P_\alpha(1,2), \quad (15)$$

where each cluster operator $\hat{f}^2(1,2)\mathcal{X}^{(n)}(1,2;i)$ is expressed in terms of products of h_α functions and τ^α projection operators and correlates the two interacting particles 1 and 2 with the other $n-2$ particles in the medium. A similar expression is obtained for the quantity $\hat{F}_{JL}^\dagger \hat{H} \hat{F}_{JL}$ appearing in the numerator of Eq. (9), where $\hat{f}^2(1,2)$ is substituted by $\hat{f}(1,2)\hat{H}(1,2)\hat{f}(1,2)$, with $\hat{H}(1,2)$ including the potential energy operator $v_4(1,2)$, and the kinetic energy operators: $\nabla_1^2 \hat{f}(1,2)$, $\nabla_1 \hat{f}(1,2)\cdot\nabla_1 \hat{f}(1,i)$, $\nabla_1 \hat{f}(1,2)\cdot\nabla_1|n]$, etc.

Inserting the cluster decomposition of Eq. (15) into Eq. (9), each cluster operator $\hat{f}^2(1,2)\mathcal{X}^{(n)}(1,2;i)$ gets multiplied by the n-body Fermi gas distribution $g_n(1,\dots,n)$. In Appendix B, the distribution $g_n(1,\dots,n)$ is expressed in terms of the uncorrelated one-body density matrix (also called the exchange

function) $\ell_N(i,j)$ and $\ell_P(i,j)$ which are given by

$$\ell_N(i,j) = \frac{1}{\rho}\sum_{n=1}^{N}\phi_n^*(i)\phi_n(j) = \ell_N(\mathbf{r}_{ij}) \sum_{m=\text{up,down}} \chi_m^*(i)\chi_m(j),$$
$$\ell_P(i,j) = \frac{1}{\rho}\sum_{n=1}^{Z}\phi_n^*(i)\phi_n(j) = \ell_P(\mathbf{r}_{ij}) \sum_{m=\text{up,down}} \chi_m^*(i)\chi_m(j), \tag{16}$$

where the sum is extended over the occupied states. They are normalized to ρ_N and ρ_P, respectively. It is useful to define a four-component vector function $\mathbf{l}(r_{ij})$ given by

$$\ell_{NN}(\mathbf{r}_{ij}) = \ell_N(\mathbf{r}_{ij}), \quad \ell_{PP}(\mathbf{r}_{ij}) = \ell_P(\mathbf{r}_{ij}),$$
$$\ell_{NP}(\mathbf{r}_{ij}) = \ell_{PN}(\mathbf{r}_{ij}) = 0. \tag{17}$$

The net result is that $\hat{f}^2(1,2)\mathcal{X}^{(n)}(1,2;i)$ gives rise to a sum of n-body *cluster integrals*, whose integrands are products of dynamical correlation functions $h_\alpha(\mathbf{r}_{ij})$ and exchange correlations $\ell_\alpha(\mathbf{r}_{ij})$.

A very important property of the FR cluster expansion, when applied to finite systems, is that in both the numerator and denominator of the diagonal matrix element of Eq. (9), the summation over the cluster integrals can be extended beyond the order A, which is the maximum for a system of A nucleons. In fact it can be extended up to infinity because any $g_n(1,\ldots,n)$ built with the exchange functions $\ell_\alpha(\mathbf{r}_{ij})$ given in Eq. (16), with $n > A$ vanishes. This property enables us to use all of the FR cluster expansion properties which are valid for a system with an unlimited number of nucleons, such as for instance nuclear matter.

More details about the FR decomposition can be found in Ref. [23]. We report here only its main properties so as to help the reader get a quick understanding of the original papers.

Each cluster integral is most conveniently represented by a *cluster diagram*. These diagrams are built by following a few convenient rules [22]:

(i) Each point represents a particle. Filled points—or internal points—represent in-medium particles while unfilled points represent external interacting particles.
(ii) Two points are linked either by a dashed line, representing $h^\alpha(\mathbf{r})$ or by a solid oriented line, representing $\ell(\mathbf{r})$ or by both.
(iii) Any internal point is reached by one or more dashed lines; two dashed lines cannot be superimposed.
(iv) Solid lines form closed loops and different loops cannot have any common point.
(v) Each internal point carries a proton or neutron density factor, depending on which type of particle it represents.
(vi) All of the particles belonging to an exchange loop are in the same spin-isospin state. Each loop (except for those comprising two particles) is counted twice, because there is one oriented clockwise and one anticlockwise. The two-particle loops are counted only once. In addition, one has to sum over loops of different spin-isospin states. The loop sign is given by $(-)^{n+1}$, where n is the number of points on the loop. The global factor C_n of an n-particle loop in spin-symmetric matter is given by

$$C_n = (-)^{n+1} \times 2 \times 2 \times \left(\rho_P^n + \rho_N^n\right)\left(\frac{1}{2}\right)^n, \tag{18}$$

where ρ_P and ρ_N are the proton and neutron matter densities, respectively. For symmetric nuclear matter ($\rho_P = \rho_N = \rho/2$), the factor C_n becomes $(-)^{n+1}8(\rho/4)^n$.

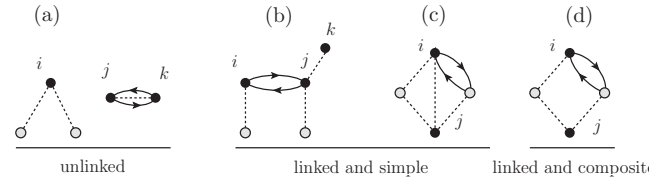

FIG. 2. Examples of cluster diagrams: (a) unlinked, (b) nodal, (c) elementary, and (d) composite. All the points correspond to neutrons.

There are some exceptions to these rules, which occur in the calculation of the expectation values of the $\tau_1 \cdot \tau_2$ and $(\sigma_1 \cdot \sigma_2)(\tau_1 \cdot \tau_2)$ potential terms. These will be discussed later, in connection with the calculation of the energy per particle.

The linked cluster theorem [22] holds also in the case of the JL-correlated basis. This theorem states that nonlinked cluster diagrams (i.e., diagrams which are built from two or more completely unconnected parts and which diverge in the thermodynamic limit) cancel exactly between the numerator and denominator of Eq. (9) so that one is then left with a series of linked cluster diagrams.

Examples of cluster diagrams are shown in Fig. 2. Diagram (a) of Fig. 2 is unlinked and is therefore forbidden. The remaining diagrams are all allowed. In the calculation of the expectation value of the scalar component of the two-body potential diagram, [Fig. 2(b)] corresponds to the following contribution:

$$\text{Diagram (1b)} \rightarrow \frac{1}{2\rho_N}\rho_N^5 \int d\mathbf{r}_{12} d\mathbf{r}_i d\mathbf{r}_j d\mathbf{r}_k f_\parallel^2(\mathbf{r}_{12}) v^c(\mathbf{r}_{12}) \times h_\parallel(\mathbf{r}_{1i}) h_\parallel(\mathbf{r}_{2j}) h_\parallel(\mathbf{r}_{jk}) \left(\frac{-\ell_N^2(\mathbf{r}_{ij})}{2}\right). \tag{19}$$

Linked cluster diagrams are subdivided into two classes: simple and composite (or hyper-chain). Simple diagrams are further classified as nodal (or chain) or elementary.

Nodal diagrams (N diagrams) are defined as diagrams having one or more *nodes*: internal (filled) points that are necessarily crossed by any path going from one interacting point to the other. For instance, diagram (b) of Fig. 2 is nodal and the points labeled with i and j are both nodes. Not-nodal diagrams (X diagrams) include both the elementary (E diagrams) and the composite ones. Composite diagrams are obtained by combining two or more nodal diagrams. Diagram (d) of Fig. 2 is composite and is composed of two nodal subdiagrams. Elementary diagrams (E diagrams) are the remaining ones. They are neither composite nor nodal. They can be constructed by first identifying the basic topological structures we want to include. Such basic structures have the property that each of their internal points is reached by at least three links and the two external points by at least two.

The links are building blocks given by $N + X$ diagrams. The basic structures are characterized by their number of points, the minimum being four (E_4). Diagram (c) of Fig. 2 is an example of four-point elementary diagrams.

V. PB-FHNC SCHEME

The PB-FHNC integral-equation method [23] gives an easy way of summing the series of cluster terms by specifying rules for building diagrams, using other diagrams as building blocks in an iterative way. The method extends hypernetted chain (HNC) theory to the case of correlated quantum Fermi systems; HNC theory was widely used in statistical thermodynamics [24] and, more recently, was applied to CBF calculations for low-temperature Bose systems such as liquid ^{4}He and ^{3}He impurity in ^{4}He [25]. It is based on two basic algorithms: the chain and hyperchain.

a. Chain algorithm. This consists of summing up the whole series of N diagrams made from a given building block. One simply takes the sum of the geometric series of the Fourier transforms of the building block function, which is given by a subset of X functions,

$$\tilde{N}(\mathbf{k}) = \rho\tilde{X}^2(\mathbf{k}) + \rho^2\tilde{X}^3(\mathbf{k}) + \cdots = \frac{\rho\tilde{X}(\mathbf{k})}{1-\rho\tilde{X}(\mathbf{k})}, \quad (20)$$

which can be expressed in terms of the following integral equation:

$$N(\mathbf{r}_{ij}) = \rho \int d\mathbf{r}_{kj} X(\mathbf{r}_{ik})(N(\mathbf{r}_{kj}) + X(\mathbf{r}_{kj})). \quad (21)$$

This formula can be interpreted in terms of probabilities. Each integral can be thought of, given two external particles i, j, as the probability to find a third in-medium particle k—expressed by ρ—times the probability of i interacting with k times the probability of k interacting with j.

b. Hyperchain algorithm. This consists of summing up the whole class of X diagrams made from a given subset of N diagrams:

$$X(\mathbf{r}_{ij}) = f^2(\mathbf{r}_{ij}) \exp\left[N(\mathbf{r}_{ij}) + E(\mathbf{r}_{ij})\right] - N(\mathbf{r}_{ij}) - 1, \quad (22)$$

where $f^2(\mathbf{r}_{ij})$ is given by $\exp(-V(\mathbf{r}_{ij})/KT)$ in statistical thermodynamics and by the correlation function of the scalar Jastrow ansatz $\prod(f(\mathbf{r}_{ij}))$ in the variational calculations of zero-temperature Bose systems. The function $E(\mathbf{r}_{ij})$ corresponds to the E diagrams, which cannot be calculated in a closed form, like the N and X diagrams. The meaning of X becomes clear if we imagine expanding the exponential in series: We are summing an increasing number of N and E diagrams. The result of this procedure will give of course composite and elementary diagrams. In addition to those the exponential term includes the nodal diagrams and the identity which we must subtract to get the sum of the not-nodal diagrams. The function $E(\mathbf{r}_{ij})$ is a functional of $N(\mathbf{r}_{ij})$ and $X(\mathbf{r}_{ij})$ and in general it is approximated by the first few-body basic diagrams (the lowest of which is the four-body basic diagram, like the diagrammatic structure underlying diagram 2(c).

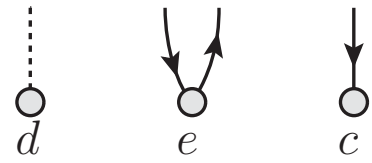

FIG. 3. Labeling of external points. See text for further details.

c. FHNC algorithm. Equations (21) and (22) are formally identical to the HNC equations of statistical thermodynamics and can be solved in an iterative way by means of the following steps:

(i) Take $N(\mathbf{r}_{ij}) = 0$.
(ii) Compute $X(\mathbf{r}_{ij})$ using Eq. (22) and taking the function $N(\mathbf{r}_{ij})$ from the previous step.
(iii) Compute $N(\mathbf{r}_{ij})$ using Eq. (21) and taking the functions $X(\mathbf{r}_{ij})$ and $N(\mathbf{r}_{ij})$ on the right-hand side from steps 2 and 3, respectively.
(iv) Return to step 2, and continue until convergence is obtained.[2]

The pair correlation function,

$$g(\mathbf{r}_{12}) = \frac{A(A-1)}{\rho^2} \frac{\int d\mathbf{r}_3 d\mathbf{r}_4 \cdots |\Psi|^2}{\int d\mathbf{r}_1 d\mathbf{r}_2 \cdots |\Psi|^2}, \quad (23)$$

where

$$\begin{aligned} g(\mathbf{r}_{12}) &= 1 + N(\mathbf{r}_{12}) + X(\mathbf{r}_{12}) \\ &= f^2(\mathbf{r}_{12}) \exp(N(\mathbf{r}_{12}) + E(\mathbf{r}_{12})). \end{aligned} \quad (24)$$

In the case of Fermi systems, in addition to the dynamical correlation bonds, there are also the exchange bonds, with the diagrammatic rules given in Sec. IV. Because of this, the FHNC method requires further subdivision of diagrams by labeling the exchange character of the two external points (e.g., Fig. 3). Each point in a diagram is labeled with a d unless it is reached by an exchange line part of a closed loop (labeled with e). Therefore, one has four different nodal functions $N_{dd}(\mathbf{r}_{ij})$, $N_{de}(\mathbf{r}_{ij})$, $N_{ed}(\mathbf{r}_{ij})$, and $N_{ee}(\mathbf{r}_{ij})$, with $N_{de}(\mathbf{r}_{ij}) = N_{ed}(\mathbf{r}_{ji})$. Similarly one has four X and E functions. In addition, one needs to introduce another class of functions, those in which the two external points are joined by an open loop of exchange lines, which are denoted with the label cc. This last class of points should not be present in allowed diagrams: Diagrams with c points are nonphysical (i.e., they have no physical meaning if taken alone) but we include them as useful building blocks to construct a diagram having a closed loop passing through the two external points 1 and 2.

It should be noticed that, as in HNC theory, the *external points* i and j of N, X, and E diagrams summed up at a given iteration of the FHNC scheme, may become internal points of the next generation of diagrams. The *true external points* 1 and 2 are those at convergence.

The chain algorithm for a Fermi system has to take into account the statistical nature of the convolution node, which

[2] If convergence cannot be achieved one can mix the newly computed functions with those computed during the previous iteration.

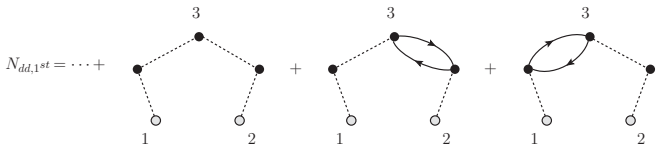

FIG. 4. Building of an N_{dd}: graphical counterpart to Eq. (25).

can be either d or e in the case of the chain equations for N_{dd}, N_{de}, and N_{ee}, and has to be necessarily of the type c for N_{cc}. As an example, the equation used to build $N_{dd}(\mathbf{r}_{ij})$ is

$$\begin{aligned} N_{dd}(\mathbf{r}_{ij}) = \rho \int_\Omega d\mathbf{r}_{kj} X_{dd}(\mathbf{r}_{ik})[X_{dd}(\mathbf{r}_{kj}) + N_{dd}(\mathbf{r}_{kj})] \\ + \rho \int_\Omega d\mathbf{r}_{kj} X_{dd}(\mathbf{r}_{ik})[X_{ed}(\mathbf{r}_{kj}) + N_{ed}(\mathbf{r}_{kj})] \\ + \rho \int_\Omega d\mathbf{r}_{kj} X_{de}(\mathbf{r}_{ik})[X_{dd}(\mathbf{r}_{kj}) + N_{dd}(\mathbf{r}_{kj})], \end{aligned} \quad (25)$$

where in the first convolution integral the node is of the d type and, in the remaining two, it is of type e. Figure 4 exemplifies the above chain equation.

In close analogy with HNC theory, the equation used to build an X_{dd} diagram is

$$X_{dd}(\mathbf{r}_{12}) = g_{dd}(\mathbf{r}_{12}) - N_{dd}(\mathbf{r}_{12}) - 1, \quad (26)$$

where

$$g_{dd}(\mathbf{r}_{12}) = f^2(\mathbf{r}_{12}) \exp(N_{dd}(\mathbf{r}_{12}) + E_{dd}(\mathbf{r}_{12})). \quad (27)$$

The complete set of formulas that are needed to compute the pair distribution function and the energy per particle are given in Ref. [23]. At present we do not know any formula able to give us a useful prescription to sum E diagrams in a closed form, like those for N and X. Luckily enough their contribution was shown to be almost negligible in the case of translationally invariant nuclear systems [26]. This allows us to neglect them for all practical purposes and hence to use the so-called FHNC/0 approximation.

A. Vertex corrections

Linked diagrams can be divided into two classes: (i) reducible diagrams [like diagram (b) of Fig. 2] having one or more *reducibility* points, which are the only contact points of two subdiagrams; (ii) irreducible diagrams [like diagrams (c) and (d) of Fig. 2] which have no reducibility points. The cluster integral corresponding to reducible diagrams is factorizable in the product of the cluster integrals corresponding to the underlying irreducible diagrammatic structures. The FHNC scheme sketched in the previous section sums up the irreducible diagrams only. In fact, they are the only remaining diagrams in pure Jastrow theory ($f_\parallel = f_\perp$), because all the reducible ones cancel each other exactly. For instance, diagrams a and b of Fig. 5 cancel each other because the exchange loop insertion leads to a factor -1 because of the orthonormality of the single-particle orbitals ϕ_n. However, the cancellation is no longer true in the more general case of the ansatz given in Eq. (10) and in Eq. (13) or when the Slater determinant of plane waves is substituted by a BCS wave function to describe

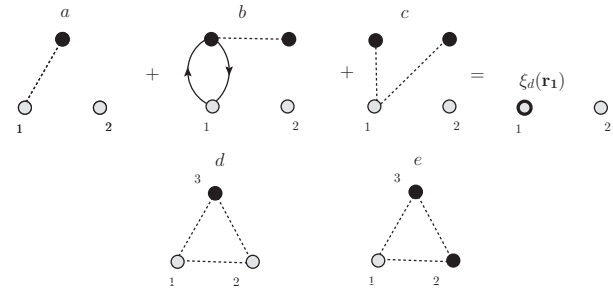

FIG. 5. Diagrammatic exemplification of vertex correction. Diagrams (a)–(c) are summed up to give $\xi_d(\mathbf{r_1})$. Diagrams (d) and (e) show a basic property of the FHNC equations for U_d and U_e. They are the same under integration. However diagram (e) contrary to diagram (d) is invariant under the exchange P_{23}. Hence, it has to be weighted with a prefactor $1/2$. That is why in the explicit formula for U_d one has to subtract from $\int d\mathbf{r}_{ij} X_{dd}(\mathbf{r}_{ij})$ several other terms that are needed to remove the overcounting coming from these missing prefactors (see Ref. [22]).

a superfluid Fermi system like, for instance, neutron matter at low density and zero temperature.

It was proved [22] that one can still use the FHNC scheme previously described, paying the price of renormalizing the various points of the irreducible diagrams by proper vertex corrections, which take into account all the possible one-body subdiagrams that can be linked to them. The process is exemplified by the diagrammatic equation displayed in Fig. 5. There are two types of vertex corrections, $\xi_d(\mathbf{r})$ for points not reached by exchange lines and $\xi_e(\mathbf{r})$ for the others. They are given by the following equations:

$$\xi_d(\mathbf{r}) = (1 + U_e(\mathbf{r})) \exp(U_d(\mathbf{r})), \quad \xi_e(\mathbf{r}) = \exp(U_d(\mathbf{r})), \quad (28)$$

where U_e and U_d are the sums of diagrams with e and d starting points, respectively. In practice, this is accomplished by integrating the functions $X_{dd}(\mathbf{r_{ij}})$ and $X_{de}(\mathbf{r_{ij}})$ over $\mathbf{r_j}$ for U_d and $X_{ed}(\mathbf{r_{ij}})$ and $X_{ee}(\mathbf{r_{ij}})$ over $\mathbf{r_j}$ for U_e and then correcting them to avoid overcounting that would arise because of the increased symmetry passing from a two-body diagram to a one-body one. For instance, triangular diagrams of Fig. 5 have different symmetry factors. The factor is 1 for the two-body diagram d of Fig. 5 and $1/2$ for the one-body diagram e of Fig. 5. The derivation of the equations leading to U_d and U_e can be found in Ref. [22]

In the above equations U_d comes in the exponential to account for the unlimited number of U_d terms that can stem

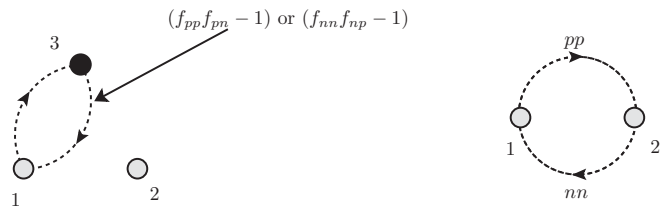

FIG. 6. (Left panel) Diagram showing how the new δ correlation results from the isospin-state flip of a particle. (Right panel) An exchange loop passing through two different external points.

from any point either of type d or type e. On the contrary, one can have one U_e term only as a vertex correction of a point of type d. It should be noted that ξ_d corresponds to the sum of all the possible one-body linked diagrams and, hence, to the one-body correlation function that, for a homogeneous system, is $g_1(r) = 1$. The sum rule $\xi_d = 1$ can be used as a measure of the accuracy of the FHNC approximation.

As a final remark, we should note that vertex corrected (or renormalized) diagrams do not need to obey our third FHNC rule (i.e., there may be diagrams with internal points not reached by a dashed line). However, this requires that the point should have been reached by a dashed line pertaining to a subdiagram accounted for by a correction, implying that we will introduce a third correction ξ_c that includes the same diagrams as ξ_e except for the identity:

$$\xi_c = \xi_e - 1. \tag{29}$$

After having sketched the main instruments of PB-FHNC theory we extend it in the following to include longitudinal isospin dependence in the correlation operator and to the $N \neq Z$ trial functions.

VI. STATE-DEPENDENT PB-FHNC EQUATIONS

The PB-FHNC equations derived in this paper are obtained for the more general form of the correlation operator, given in Eq. (11) and not for the restricted one of Eq. (13). It follows that nodal, composite, elementary functions, as well as distribution functions, will have the structure of a four-component vector,

$$\mathbf{A}(\mathbf{r}_{ij}) = (A^{NN}(\mathbf{r}_{ij}), A^{PP}(\mathbf{r}_{ij}), A^{NP}(\mathbf{r}_{ij}), A^{PN}(\mathbf{r}_{ij})), \tag{30}$$

where we have also indicated the projectors used in Eq. (13).

Our nodal equations can be written in a compact way by exploiting the convolution formalism. We make the definition:

$$\mathbf{C}_\alpha(\mathbf{r}_{ij}) = (\mathbf{A}(\mathbf{r}_{ik}) \,|\, \mathbf{B}(\mathbf{r}_{kj}))_\alpha, \tag{31}$$

where the subscript α denotes the exchange nature of the node k and, consequently, that of the related vertex correction. It can be of type d, e, or c. The four components of $\mathbf{C}$ are given by

$$\begin{aligned}
C_\alpha^{NN}(\mathbf{r}_{ij}) &= \sum_{b=N,P} \rho_b \xi_\alpha^b \int_\Omega d\mathbf{r}_k A^{Nb}(\mathbf{r}_{ik}) B^{bN}(\mathbf{r}_{kj}),\\
C_\alpha^{PN}(\mathbf{r}_{ij}) &= \sum_{b=N,P} \rho_b \xi_\alpha^b \int_\Omega d\mathbf{r}_k A^{Pb}(\mathbf{r}_{ik}) B^{bN}(\mathbf{r}_{kj}),\\
C_\alpha^{NP}(\mathbf{r}_{ij}) &= \sum_{b=N,P} \rho_b \xi_\alpha^b \int_\Omega d\mathbf{r}_k A^{Nb}(\mathbf{r}_{ik}) B^{bP}(\mathbf{r}_{kj}),\\
C_\alpha^{PP}(\mathbf{r}_{ij}) &= \sum_{b=N,P} \rho_b \xi_\alpha^b \int_\Omega d\mathbf{r}_k A^{Pb}(\mathbf{r}_{ik}) B^{bP}(\mathbf{r}_{kj}).
\end{aligned} \tag{32}$$

1. Nodal diagrams

Using the above convolution formalism the chain equations for $\mathbf{N}_{dd}$, $\mathbf{N}_{de}$, $\mathbf{N}_{ed}$, and $\mathbf{N}_{ee}$ can be recast in a more compact way, as follows:

$$\begin{aligned}
\mathbf{N}_{dd} &= (\mathbf{X}_{dd} \,|\, \mathbf{N}_{dd} + \mathbf{X}_{dd})_d + (\mathbf{X}_{de} \,|\, \mathbf{N}_{dd} + \mathbf{X}_{dd})_e \\
&\quad + (\mathbf{X}_{dd} \,|\, \mathbf{N}_{ed} + \mathbf{X}_{ed})_e, \\
\mathbf{N}_{de} &= (\mathbf{X}_{dd} \,|\, \mathbf{N}_{de} + \mathbf{X}_{de})_d + (\mathbf{X}_{de} \,|\, \mathbf{N}_{de} + \mathbf{X}_{de})_e \\
&\quad + (\mathbf{X}_{dd} \,|\, \mathbf{N}_{ee} + \mathbf{X}_{ee})_e, \\
\mathbf{N}_{ed} &= (\mathbf{X}_{ed} \,|\, \mathbf{N}_{dd} + \mathbf{X}_{dd})_d + (\mathbf{X}_{ee} \,|\, \mathbf{N}_{dd} + \mathbf{X}_{dd})_e \\
&\quad + (\mathbf{X}_{ed} \,|\, \mathbf{N}_{ed} + \mathbf{X}_{ed})_e, \\
\mathbf{N}_{ee} &= (\mathbf{X}_{ed} \,|\, \mathbf{N}_{de} + \mathbf{X}_{de})_d + (\mathbf{X}_{ee} \,|\, \mathbf{N}_{de} + \mathbf{X}_{de})_e \\
&\quad + (\mathbf{X}_{ed} \,|\, \mathbf{N}_{ee} + \mathbf{X}_{ee})_e.
\end{aligned} \tag{33}$$

The chain equation for $\mathbf{N}_{cc}$ can be written in convolution notation as

$$\begin{aligned}
\mathbf{N}_{cc}(\mathbf{r}_{12}) &= \left(\mathbf{X}_{cc} \,|\, \mathbf{X}_{cc} + \mathbf{N}_{cc} - \frac{\mathbf{l}}{d}\right)_e + \left(-\frac{\mathbf{l}}{d}\middle|\, \mathbf{X}_{cc} + \mathbf{P}\right)_e \\
&\quad + \left(-\frac{\mathbf{l}}{d}\middle|\, -\frac{\mathbf{l}}{d} + \mathbf{N}_{cc} - \mathbf{P}\right)_c,
\end{aligned} \tag{34}$$

where $\mathbf{P}$ is given by

$$\mathbf{P}(\mathbf{r}_{12}) = \left(\mathbf{X}_{cc} \,|\, \mathbf{X}_{cc} + \mathbf{N}_{cc} - \frac{\mathbf{l}}{d}\right)_e. \tag{35}$$

These last two equations cannot, however, be applied blindly. According to the RF definitions, cc diagrams have exchange-line paths connecting 1 directly to 2 and so, since exchange correlations cannot flip spins, only PP and NN components are allowed,whereas the components NP and PN vanish for N_{cc}, X_{cc}, E_{cc}, and P. The degeneracy factor (d) here is equal to 2, accounting only for the two possible spin states (the isospin states of a pair are singled out in our treatment).

2. Composite diagrams

The equations for the composite functions are a straightforward generalization of the corresponding equations in standard PB-FHNC theory, and are given by

$$\begin{aligned}
X_{dd}^\alpha(\mathbf{r}_{12}) &= g_{dd}^\alpha(\mathbf{r}_{12}) - N_{dd}^\alpha(\mathbf{r}_{12}) - 1, \\
X_{de}^\alpha(\mathbf{r}_{12}) &= X_{ed}^\alpha(\mathbf{r}_{21}) = g_{dd}^\alpha(\mathbf{r}_{12})\left[N_{de}^\alpha(\mathbf{r}_{12}) + E_{de}^\alpha(\mathbf{r}_{12})\right] \\
&\quad - N_{de}^\alpha(\mathbf{r}_{12}), \\
X_{ee}^\alpha(\mathbf{r}_{12}) &= g_{dd}^\alpha(\mathbf{r}_{12})\Bigg\{N_{ee}^\alpha(\mathbf{r}_{12}) + E_{ee}^\alpha(\mathbf{r}_{12}) \\
&\quad + \left[N_{de}^\alpha(\mathbf{r}_{12}) + E_{de}^\alpha(\mathbf{r}_{12})\right]^2 - d\Bigg[N_{cc}^\alpha(\mathbf{r}_{12}) \\
&\quad - \frac{1}{d}\ell_\alpha(\mathbf{r}_{12}) + E_{cc}^\alpha(\mathbf{r}_{12})\Bigg]^2\Bigg\} - N_{ee}^\alpha(\mathbf{r}_{12}), \\
X_{cc}^\alpha(\mathbf{r}_{12}) &= g_{dd}^\alpha(\mathbf{r}_{12})\left[N_{cc}^\alpha(\mathbf{r}_{12}) - \tfrac{1}{2}\ell_a(\mathbf{r}_{12}) + E_{cc}^\alpha(\mathbf{r}_{12})\right] \\
&\quad - N_{cc}^\alpha(\mathbf{r}_{12}) + \tfrac{1}{2}\ell_\alpha(\mathbf{r}_{12}),
\end{aligned} \tag{36}$$

where the g_{dd} distribution function is defined as

$$g_{dd}^\alpha(\mathbf{r}_{12}) = f^{\alpha 2}(\mathbf{r}_{12}) \exp\left[N_{dd}^\alpha(\mathbf{r}_{12}) + E_{dd}^\alpha(\mathbf{r}_{12})\right]. \tag{37}$$

It is useful to define also the following four distribution functions:

$$\begin{aligned} g^{\alpha}_{de}(\mathbf{r}_{12}) &= g^{\bar{\alpha}}_{ed}(\mathbf{r}_{21}) = N^{\alpha}_{de}(\mathbf{r}_{12}) + X^{\alpha}_{de}(\mathbf{r}_{12}), \\ (g_{\rm dir})^{\alpha}_{ee}(\mathbf{r}_{12}) &= g^{\alpha}_{dd}(\mathbf{r}_{12})\big\{N^{\alpha}_{ee}(\mathbf{r}_{12}) + (E_{\rm dir})^{\alpha}_{ee}(\mathbf{r}_{12}) \\ &\quad + \big[N^{\alpha}_{de}(\mathbf{r}_{12}) + E^{\alpha}_{de}(\mathbf{r}_{12})\big]^2\big\} - N^{\alpha}_{ee}(\mathbf{r}_{12}), \\ (g_{\rm exch})^{\alpha}_{ee}(\mathbf{r}_{12}) &= -d\, g^{\alpha}_{dd}(\mathbf{r}_{12})\bigg[N^{\alpha}_{cc}(\mathbf{r}_{12}) - \frac{1}{d}\ell_a(\mathbf{r}_{12}) \\ &\quad + E^{\alpha}_{cc}(\mathbf{r}_{12})\bigg]^2 + g^{\alpha}_{dd}(E_{\rm exch})^{\alpha}_{ee}(\mathbf{r}_{12}), \\ g^{\alpha}_{cc}(\mathbf{r}_{12}) &= N^{\alpha}_{cc}(\mathbf{r}_{12}) + X^{\alpha}_{cc}(\mathbf{r}_{12}) - \frac{1}{d}\ell_{\alpha}(\mathbf{r}_{12}), \end{aligned} \tag{38}$$

where the components $\alpha = NP$ and $\alpha = PN$ of $(g_{\rm exch})_{ee}$ are identically zero.

3. Vertex corrections

In deriving the vertex corrections we need to distinguish whether the vertex to be corrected is a neutron or a proton. Extending the derivation of Ref. [22] we get the following expressions:

$$\begin{aligned} U^N_d = \sum_{b=N,P}\rho_b\int_{\Omega} d\mathbf{r}_{12}\big\{&\xi^b_d\big[X^{Nb}_{dd}(\mathbf{r}_{12}) - E^{Nb}_{dd}(\mathbf{r}_{12}) \\ &- S^{Nb}_{dd}(\mathbf{r}_{12})\big(g^{Nb}_{dd}(\mathbf{r}_{12}) - 1\big)\big] + \xi^b_e\big[X^{Nb}_{de}(\mathbf{r}_{12}) - E^{Nb}_{de}(\mathbf{r}_{12}) \\ &- S^{Nb}_{dd}(\mathbf{r}_{12})g^{Nb}_{de}(\mathbf{r}_{12}) - S^{Nb}_{de}(\mathbf{r}_{12})\big(g^{Nb}_{dd}(\mathbf{r}_{12}) - 1\big)\big]\big\} + E^n_d, \end{aligned} \tag{39}$$

for the vertex correction of type d, and

$$\begin{aligned} U^N_e = \sum_{b=N,P}\rho_b\int_{\Omega} d\mathbf{r}_{12}\big\{&\xi^b_d\big[X^{Nb}_{ed}(\mathbf{r}_{12}) - E^{Nb}_{ed}(\mathbf{r}_{12})\big] + \xi^b_e\big[X^{Nb}_{ee}(\mathbf{r}_{12}) - E^{Nb}_{ee}(\mathbf{r}_{12})\big] - \xi^b_d\big[S^{Nb}_{dd}(\mathbf{r}_{12})g^{Nb}_{ed}(\mathbf{r}_{12}) + S^{Nb}_{ed}(\mathbf{r}_{12})g^{Nb}_{dd}(\mathbf{r}_{12})\big] \\ &- \xi^b_e\big[S^{Nb}_{ee}(\mathbf{r}_{12})\big(g^{Nb}_{dd}(\mathbf{r}_{12}) - 1\big) + S^{Nb}_{ed}(\mathbf{r}_{12})g^{Nb}_{de}(\mathbf{r}_{12}) + S^{Nb}_{de}(\mathbf{r}_{12})g^{Nb}_{ed}(\mathbf{r}_{12}) + S^{Nb}_{dd}(\mathbf{r}_{12})g^{Nb}_{ee}(\mathbf{r}_{12})\big]\big\} \\ - d\int_{\Omega} d\mathbf{r}_{12}\bigg\{&\rho_N\xi^N_e S^{NN}_{cc}(\mathbf{r}_{12})g^{NN}_{cc}(\mathbf{r}_{12}) + \ell_N(\mathbf{r}_{12})\bigg[\mathcal{N}^{NN}_{cc}(\mathbf{r}_{12}) - \frac{1}{d}\ell_N(\mathbf{r}_{12})\bigg]\bigg\} + E^N_e, \end{aligned} \tag{40}$$

for the vertex correction of type e, where $\mathcal{N}$ is a shorthand for

$$\begin{aligned} \mathcal{N}^{NN}_{cc}(\mathbf{r}_{12}) = N^{NN}_{cc}(\mathbf{r}_{12}) - \xi^N_e\rho_N\int_{\Omega} d\mathbf{r}_{32}X^{NN}_{cc}(\mathbf{r}_{13})\bigg[&X^{NN}_{cc}(\mathbf{r}_{32}) \\ &+ N^{NN}_{cc}(\mathbf{r}_{32}) - \frac{1}{d}\ell_N(\mathbf{r}_{32})\bigg], \end{aligned} \tag{41}$$

and the quantity S is defined as

$$S_{ij} = \tfrac{1}{2}(N_{ij} + E_{ij}). \tag{42}$$

Obviously $U^p_{e,d}$ is given by simply interchanging each superscript $p \leftrightarrow n$ in the above.

4. Two-body distribution function

The above equations can be solved iteratively. At convergence, the solutions can be used to compute the *scalar* two-body distribution function, given by

$$\begin{aligned} g_c(\mathbf{r}_{12}) &= \sum_{a,b=N,P} g^{ab}_c(\mathbf{r}_{12}) \\ &= \frac{1}{\rho^2}\sum_{a,b=N,P}\rho_a\rho_b\big[\xi^a_d\xi^b_d g^{ab}_{dd}(\mathbf{r}_{12}) + \xi^a_d\xi^b_e g^{ab}_{de}(\mathbf{r}_{12}) \\ &\quad + \xi^a_e\xi^b_d g^{ab}_{ed}(\mathbf{r}_{12}) + \xi^a_e\xi^b_e\big((g_{\rm dir})^{ab}_{ee}(\mathbf{r}_{12}) \\ &\quad + (g_{\rm exch})^{ab}_{ee}(\mathbf{r}_{12})\big)\big]. \end{aligned} \tag{43}$$

In the case of symmetric nuclear matter ($N = Z$) and of a state-independent correlation operator ($f_{\parallel} = f_{\perp}$), the quantity $g_c(\mathbf{r}_{12})$ recovers the two-body distribution function $g(\mathbf{r}_{12})$ of Jastrow theory given in Eq. (24). This can be easily understood by taking into account (i) the sum rule $\xi_d = 1$ and (ii) that $\xi_e g_{de}$ and $\xi^2_e g_{ee}$ of our vertex corrected PB-FHNC theory coincide with the corresponding distribution functions g_{de} and g_{ee} of the standard one.

A. Potential energy expectation value

The expectation value of a two-body potential of the v_4 type on the trial function $\hat{F}_{JL}|0]$ is given by

$$\begin{aligned} \frac{\langle V\rangle}{A} = \frac{\rho}{2}\int_{\Omega} d\mathbf{r}_{12}\{&v_c(\mathbf{r}_{12})g_c(\mathbf{r}_{12}) + 3v_{\sigma}(\mathbf{r}_{12})g_{\sigma}(\mathbf{r}_{12}) \\ &+ v_{\tau}(\mathbf{r}_{12})g_{\tau}(\mathbf{r}_{12}) + 3v_{\sigma\tau}(\mathbf{r}_{12})g_{\sigma\tau}(\mathbf{r}_{12})\}. \end{aligned} \tag{44}$$

The first term on the right-hand side corresponds to the expectation value of the scalar component of the v_4 potential. We discuss, in the following, the remaining three terms. Recall that we are dealing with a polarized system with respect to isospin ($N \neq Z$), but with a strictly nonpolarized one with respect to spin.

1. $\sigma_1 \cdot \sigma_2$ term

The correlation operator $\hat{F}_{JL}$ has no spin dependence. Since $\langle \sigma_1 \cdot \sigma_2\rangle = 0$ in spin symmetrical matter, in the calculation of the expectation value of $v_{\sigma}(\mathbf{r}_{12})\sigma_1 \cdot \sigma_2$, the *direct* terms of the distribution function do not contribute. On the contrary, the exchange terms carry the spin-exchange operator and one has

to take care of the following spin algebra

$$\langle(\sigma_1\cdot\sigma_2)P_\sigma(1,2)\rangle = \left\langle(\sigma_1\cdot\sigma_2)\frac{1+\sigma_1\cdot\sigma_2}{2}\right\rangle = \left\langle\frac{3-\sigma_1\cdot\sigma_2}{2}\right\rangle = \frac{3}{2}. \quad (45)$$

In conclusion we have

$$g_\sigma(\mathbf{r}_{12}) = \frac{1}{\rho^2}\Big(\big(\xi_e^N\rho_N\big)^2(g_{\rm exch})_{ee}^{NN}(\mathbf{r}_{12}) + (\xi_e^P\rho^P)^2(g_{\rm exch})_{ee}^{PP}(\mathbf{r}_{12})\Big). \quad (46)$$

2. $\tau_1\cdot\tau_2$ term

The operator $\tau_1\cdot\tau_2$ carried by the τ component of the $\hat{v}_4$ potential requires a specific and new PB-FHNC treatment, when dealing with a correlation operator of the $\hat{F}_{JL}$ type and a $N\neq Z$ matter. We begin by calculating the isospin matrix elements.

The direct terms are

$$\begin{aligned}\langle NN\,|\,v_\tau(\tau_1\cdot\tau_2)\,|\,nNN\rangle &= \langle PP\,|\,v_\tau(\tau_1\cdot\tau_2)\,|\,PP\rangle = v_\tau(\mathbf{r}_{12}),\\ \langle NP\,|\,v_\tau(\tau_1\cdot\tau_2)\,|\,NP\rangle &= \langle PN\,|\,v_\tau(\tau_1\cdot\tau_2)\,|\,PN\rangle = -v_\tau(\mathbf{r}_{12}),\end{aligned} \quad (47)$$

and the exchange terms are

$$\begin{aligned}\langle NN\,|\,v_\tau(\tau_1\cdot\tau_2)P_\tau\,|\,nNN\rangle &= \langle PP\,|\,v_\tau(\tau_1\cdot\tau_2)P_t au\,|\,PP\rangle = v_\tau(\mathbf{r}_{12}),\\ \langle NP\,|\,v_\tau(\tau_1\cdot\tau_2)P_\tau\,|\,NP\rangle &= \langle PN\,|\,v_\tau(\tau_1\cdot\tau_2)P_\tau\,|\,PN\rangle = 2v_\tau(\mathbf{r}_{12}).\end{aligned} \quad (48)$$

The second row of the above equation deserves particular attention. Because of the fact that we have, for example, $|\,NP\rangle$ in the ket and $\langle PN\,|$ in the bra, we have the following:

(i) A different kind of correlation reaching the *external* point 1 or the external point 2. Under the assumption of Eq. (13) there is only one type for such new correlations, and we denote it as δ correlation (See Fig. 6 left panel):

$$h_\delta(\mathbf{r}_{ij}) = f_\parallel(\mathbf{r}_{ij})f_\perp(\mathbf{r}_{ij}) - 1. \quad (49)$$

(ii) The exchange loop passing through 1 and 2 is made of two cyclic nodal functions, one of type P and the other of type N (See Fig. 6 right panel).

It follows that the g distribution for these matrix elements, which we denote by $g_\delta(\vec{r}_{12})$, has to be built by solving appropriate PB-FHNC equations, taking into account the above two properties. We have

$$g_\tau(\mathbf{r}_{12}) = \frac{1}{\rho^2}\Bigg(g_\delta(\mathbf{r}_{12}) + \sum_{a=N,P}\Big\{\rho_a^2\Big[(\xi_d^a)^2 g_{dd}^{aa}(\mathbf{r}_{12}) + \xi_d^a\xi_e^a\big(g_{de}^{aa}(\mathbf{r}_{12}) + g_{ed}^{aa}(\mathbf{r}_{12})\big) + \big(\xi_e^a\big)^2\big((g_{\rm dir})_{ee}^{aa}(\mathbf{r}_{12}) + (g_{\rm exch})_{ee}^{aa}(\mathbf{r}_{12})\big)\Big]\Big\} - \sum_{a=N,P}\rho_a\rho_{\bar a}\Big[\xi_d^a\xi_d^{\bar a}g_{dd}^{a\bar a}(\mathbf{r}_{12}) + \xi_d^a\xi_e^{\bar a}g_{de}^{a\bar a}(\mathbf{r}_{12}) + \xi_e^a\xi_e^{\bar a}g_{ed}^{a\bar a}(\mathbf{r}_{12}) + \xi_e^a\xi_e^{\bar a}(g_{\rm dir})_{ee}^{a\bar a}(\mathbf{r}_{12})\big)\Big)\Bigg), \quad (50)$$

where $\bar a$ labels the isospin conjugate of a, namely $|\,\bar a\rangle = \tau_x\,|\,a\rangle$ and the mixed distribution function g_δ is given by

$$g_\delta(\mathbf{r}_{12}) = -4d\rho_N\rho_P\xi_{e\delta}^2 f_\perp^2 e^{N_{\delta\delta}^{NP}(\mathbf{r}_{12})}\left[N_{\delta\delta cc}^{NN}(\mathbf{r}_{12}) - \frac{1}{d}\ell_N(\mathbf{r}_{12})\right]\times\left[N_{\delta\delta cc}^{PP}(\mathbf{r}_{12}) - \frac{1}{d}\ell_P(\mathbf{r}_{12})\right]. \quad (51)$$

In the case of $N=Z$ matter and $f_\parallel = f_\perp$, one has $\rho_N=\rho_P$, $\xi^N=\chi^P$ with the result that $g_\delta = 2g_\sigma$ and consequently that $g_\tau = 3g_\sigma$.

The nodal function $N_{\delta\delta}^{NP}(\mathbf{r}_{12})$ is defined by the convolution:

$$N_{\delta\delta}^{NP}(\mathbf{r}_{12}) = (\mathbf{X}_{\delta d}\,|\,\mathbf{N}_{d\delta}+\mathbf{X}_{d\delta})_d + (\mathbf{X}_{\delta e}\,|\,\mathbf{N}_{d\delta}+\mathbf{X}_{d\delta})_e + (\mathbf{X}_{\delta d}\,|\,\mathbf{N}_{e\delta}+\mathbf{X}_{e\delta})_e, \quad (52)$$

where the nodal and composite vector functions of the type $d\delta$ and $e\delta$ have only the two components which specify the isospin state of the particle related to the external label d or e. The two chain equations are

$$\begin{aligned}\mathbf{N}_{\delta d}(\mathbf{r}_{12}) &= ((\mathbf{X}_{\delta d}\,|\,(\mathbf{N}_{dd}+(\mathbf{X}_{dd})_d + ((\mathbf{X}_{\delta e}\,|\,\mathbf{N}_{dd}+\mathbf{X}_{dd})_e + (\mathbf{X}_{\delta d}\,|\,\mathbf{N}_{ed}+\mathbf{X}_{ed})_e,\\ (\mathbf{N}_{\delta e}(\mathbf{r}_{12}) &= (\mathbf{X}_{\delta d}\,|\,(\mathbf{N}_{de}+(\mathbf{X}_{de})_d + ((\mathbf{X}_{\delta e}\,|\,(\mathbf{N}_{de}+(\mathbf{X}_{de})_e + ((\mathbf{X}_{\delta d}\,|\,(\mathbf{N}_{ee}+(\mathbf{X}_{ee})_e,\end{aligned} \quad (53)$$

and the composite functions are

$$\begin{aligned}X_{\delta d}^b(\mathbf{r}_{12}) &= g_{\delta d}^b(\mathbf{r}_{12}) - N_{\delta d}^b(\mathbf{r}_{12}) - 1,\\ X_{\delta e}^b(\mathbf{r}_{12}) &= X_{e\delta}^b(\mathbf{r}_{21}) = g_{\delta d}^b(\mathbf{r}_{12})\big[N_{\delta e}^b(\mathbf{r}_{12}) + E_{\delta e}^b(\mathbf{r}_{12})\big] - N_{\delta e}^b(\mathbf{r}_{12}),\end{aligned} \quad (54)$$

with $b=N$, P, and $g_{\delta d}$ given by

$$g_{\delta d}^b(\mathbf{r}_{12}) = f_\parallel(\mathbf{r}_{12})f_\perp(\mathbf{r}_{12})e^{(N_{\delta d}^b(\mathbf{r}_{12})+X_{\delta d}^b(\mathbf{r}_{12}))}. \quad (55)$$

The two components $N_{\delta\delta cc}^\alpha$, with $\alpha = NN, PP$, entering Eq. (51), can be given in terms of the following convolution equation:

$$\mathbf{N}_{\delta\delta cc}(\mathbf{r}_{12}) = \left(\mathbf{X}_{\delta cc}\,|\,\mathbf{X}_{\delta cc}+\mathbf{N}_{\delta cc}-\frac{\mathbf{l}}{d}\right)_e + \left(-\frac{\mathbf{l}}{d}\middle|\,\mathbf{X}_{\delta cc}+\hat{P}_\delta\right)_e + \left(-\frac{\mathbf{l}}{d}\middle|-\frac{\mathbf{l}}{d}+\mathbf{N}_{\delta cc}-\mathbf{P}_\delta\right)_c, \quad (56)$$

where the two-component vector functions $\mathbf{N}_{\delta\delta cc}$, $\mathbf{X}_{\delta\delta cc}$, and $\mathbf{P}_\delta$ are given by

$$\mathbf{N}_{\delta cc}(\mathbf{r}_{12}) = \left(\mathbf{X}_{\delta cc}\,|\,\mathbf{X}_{cc}+\mathbf{N}_{cc}-\frac{\mathbf{l}}{d}\right)_e + \left(-\frac{\mathbf{l}}{d}\middle|\,\mathbf{X}_{cc}+\mathbf{P}\right)_e + \left(-\frac{\mathbf{l}}{d}\middle|-\frac{\mathbf{l}}{d}+\mathbf{N}_{cc}-\mathbf{P}\right)_c,$$

TABLE I. Results for symmetrical nuclear matter at $\rho = 0.16$ for different correlated models. The first two rows for each potential are obtained for 2060 nucleons in a periodic box by using the vertex corrected PB-FHNC equations. We have used a grid with 60 points in each direction.The third and fourth rows report the results obtained with FHNC/SOC equations in the thermodynamic limit for the $\hat{F}_2$ and $\hat{F}_4$ models. The energies are in MeV.

Potential	Approx.	A	E_{free}	PE	KE	E
$AT4'$	Jastrow	2060	22.136	−43.595	28.455	−15.150
	$\hat{F}_{JL}$	2060	22.136	−44.053	28.016	−16.090
	$\hat{F}_2$	∞	22.107	−44.163	28.208	−15.955
	$\hat{F}_4$	∞	22.107	−44.756	28.587	−16.169
$(AV8')_4$	Jastrow	2060	22.136	−27.545	29.499	1.954
	$\hat{F}_{JL}$	2060	22.136	−30.070	31.722	1.652
	$\hat{F}_2$	∞	22.108	−28.569	30.152	1.583
	$\hat{F}_4$	∞	22.108	−31.146	32.055	0.909

$$X^{\alpha}_{\delta cc}(\mathbf{r}_{12}) = g^{\alpha}_{\delta d}(\mathbf{r}_{12})\big[N^{\alpha}_{\delta cc}(\mathbf{r}_{12}) - \frac{1}{2}\ell_a(\mathbf{r}_{12}) + E^{\alpha}_{\delta cc}(\mathbf{r}_{12})\big] - N^{\alpha}_{\delta cc}(\mathbf{r}_{12}) + \frac{1}{2}\ell_a(\mathbf{r}_{12}),$$
$$\mathbf{P}_{\delta}(\mathbf{r}_{12}) = \left(\mathbf{X}_{cc}\,|\,\mathbf{X}_{cc\delta} + \mathbf{N}_{cc\delta} - \frac{\mathbf{l}}{d}\right)_e. \tag{57}$$

To complete our PB-FHNC set, we need to define U^a_{δ} so as to define $\xi^a_{\delta e}$:

$$\xi_{\delta e} = e^{U_{\delta}}, \tag{58}$$
$$U_{\delta} = \sum_{b=N,P}\rho^b\int_{\Omega} d\mathbf{r}_{12}\big\{\xi^b_d\big[X^b_{\delta d}(\mathbf{r}_{12}) - E^b_{\delta d}(\mathbf{r}_{12}) - S^b_{\delta d}(\mathbf{r}_{12})\big(g^b_{\delta d}(\mathbf{r}_{12}) - 1\big)\big] + \xi^b_e\big[X^b_{\delta e}(\mathbf{r}_{12}) - E^b_{\delta e}(\mathbf{r}_{12}) - S^b_{\delta d}(\mathbf{r}_{12})g^b_{\delta e}(\mathbf{r}_{12}) - S^b_{\delta e}(\mathbf{r}_{12})\big(g^b_{\delta d}(\mathbf{r}_{12}) - 1\big)\big]\big\} + E_{\delta}, \tag{59}$$

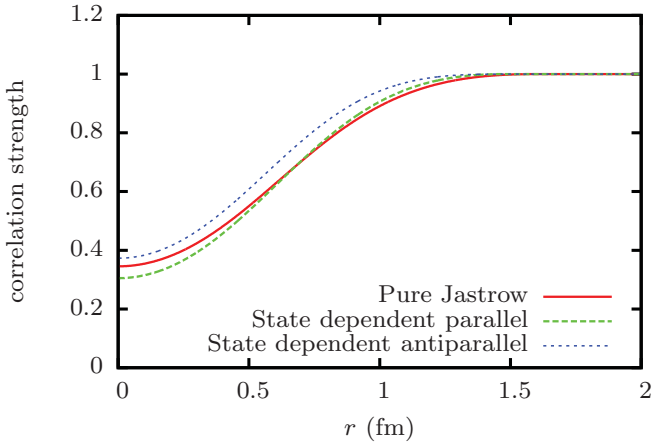

FIG. 7. (Color online) AT4′ correlation functions at $\rho = 0.16$. The parallel and antiparallel correlations of the $\hat{F}_{JL}$ model are compared with Jastrow correlation.

TABLE II. PB-FHNC Results for the $AT4'$ potential at ρ_0. For the smaller systems, 26 neighbor cells were summed over; our grid had 60 points in each direction. Δ_E gives the difference in energy with respect to the Jastrow case. The energies are in MeV.

A	E_{free}	PE	KE	E	Δ_E
28	22.427	−43.994	28.311	−15.682	−0.888
76	21.231	−44.890	27.119	−17.771	−0.938
108	21.277	−44.933	27.163	−17.769	−0.932
132	21.996	−44.304	27.895	−16.409	−0.935
2060	22.136	−44.053	28.016	−16.090	−0.940

where

$$g^b_{\delta e}(\mathbf{r}_{12}) = N^b_{\delta e}(\mathbf{r}_{12}) + X^b_{\delta e}(\mathbf{r}_{12}),$$
$$S^b_{\delta t}(\mathbf{r}_{12}) = \tfrac{1}{2}\big(N^b_{\delta t}(\mathbf{r}_{12}) + E^b_{\delta t}(\mathbf{r}_{12})\big) \quad (t = d, e). \tag{60}$$

3. $(\boldsymbol{\sigma}_1 \cdot \boldsymbol{\sigma}_2)(\boldsymbol{\tau}_1 \cdot \boldsymbol{\tau}_2)$ term

The distribution function $g_{\sigma\tau}$ can be easily calculated by using the expressions derived in the previous two subsections.

$$g_{\sigma\tau}(\mathbf{r}_{12}) = \frac{1}{\rho^2}\big(\rho^2_N\big(\xi^n_e\big)^2(g_{\text{exch}})^{NN}_{ee}(\mathbf{r}_{12}) + \rho^2_P\big(\xi^p_e\big)^2(g_{\text{exch}})^{PP}_{ee}(\mathbf{r}_{12}) + g_{\delta}\big). \tag{61}$$

B. Kinetic energy expectation value

In this section we calculate the expectation value of the kinetic energy $\langle K\rangle/A$ using the Jackson-Feenberg identity, following the procedure shown in Ref. [27] and further discussed in Ref. [22]. It is given as a sum of three terms: a term giving the Fermi energy (E_F), a term accounting for two-body contributions (E_2), and a term for three-body contributions (E_3).

The Fermi energy is easily expressed as

$$E_F = \frac{1}{N}\sum_{\text{filled } N \text{ states}}\frac{\hbar^2k^2_N}{2m} + \frac{1}{Z}\sum_{\text{filled } Z \text{ states}}\frac{\hbar^2k^2_P}{2m}. \tag{62}$$

The two-body contribution to the kinetic energy can be split into two parts: the first one accounting for the contribution coming from ∇^2 acting on the correlations $f_{\parallel}$ and $f_{\perp}$ and the second one accounting for exchanges. The resulting expression

TABLE III. Results for the $(AV8')_4$ potential at ρ_0. See captions of Table II.

A	E_{free}	PE	KE	E	Δ_E
28	22.427	−30.937	31.971	1.034	−0.270
76	21.231	−30.618	30.782	0.164	−0.250
108	21.277	−30.590	30.826	0.235	−0.249
132	21.996	−30.187	31.559	1.372	−0.256
2060	22.136	−30.070	31.722	1.652	−0.302

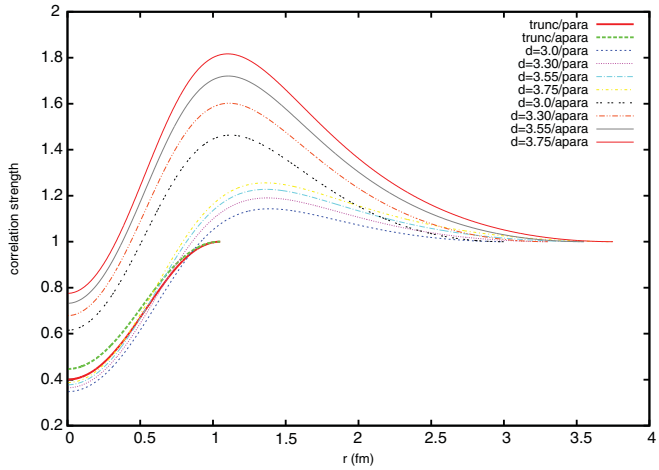

FIG. 8. (Color online) AT4′ correlation functions at $\rho = 0.016$ for different healing distances (d) either for $f_\parallel$ (marked with p) or $f_\perp$ (marked with a). We show for comparison two correlation functions whose healing distance was set to 1 so to keep their value everywhere below 1.

for the case of the $\hat{F}_{JL}$ ansatz and a $N \neq Z$ matter is

$$
\begin{aligned}
E_2 &= E_2^F + E_2^\Phi, \\
E_2^F &= -\frac{\hbar^2}{4m}\rho \int_\Omega d\mathbf{r}\left[g_c^{NN}(\mathbf{r}) + g_c^{PP}(\mathbf{r})\right]\nabla^2 \ln f_\parallel(\mathbf{r}) \\
&\quad - \frac{\hbar^2}{4m}\rho \int_\Omega d\mathbf{r}\left[g_c^{PN}(\mathbf{r}) + g_c^{NP}(\mathbf{r})\right]\nabla^2 \ln f_\perp(\mathbf{r}), \\
E_2^\Phi &= -\frac{\hbar^2}{8m}\frac{\rho_N^2}{\rho}\int_\Omega d\mathbf{r}\left(g_{dd}^{NN}(\mathbf{r}) - 1\right)\left(\frac{1}{d}\nabla^2 \ell_N{}^2(\mathbf{r})\right. \\
&\quad \left. - 2\xi_e^N N_{cc}^{NN}(\mathbf{r})\nabla^2\ell_N(\mathbf{r}) + 2\xi_c^N\frac{\ell_N}{d}\nabla^2\ell_N(\mathbf{r})\right) \\
&\quad - \frac{\hbar^2}{8m}\frac{\rho_P^2}{\rho}\int_\Omega d\mathbf{r}\left(g_{dd}^{PP}(\mathbf{r}) - 1\right)\left(\frac{1}{d}\nabla^2 \ell_P{}^2(\mathbf{r})\right. \\
&\quad \left. - 2\xi_e^P N_{cc}^{PP}(\mathbf{r})\nabla^2\ell_P(\mathbf{r}) + 2\xi_c^P\frac{\ell_P}{d}\nabla^2\ell_P(\mathbf{r})\right). \qquad (63)
\end{aligned}
$$

The three-body contribution comes from $(\nabla\ell_{12}\cdot\nabla\ell_{13})$ and is given by

$$
\begin{aligned}
E_3 = -\frac{\hbar^2}{4md}\sum_{a=N,P}\frac{\rho_a^3}{\rho}\int_\Omega d\mathbf{r}\int_\Omega d\mathbf{r}'\nabla\ell_a(\mathbf{r})\cdot\nabla\ell_a(\mathbf{r}') \\
\times\left(g_{dd}^{aa}(\mathbf{r}) - 1\right)\left(g_{dd}^{aa}(\mathbf{r}') - 1\right) \\
\times\xi_e^a\left[N_{cc}^a(\mathbf{r}-\mathbf{r}') - \frac{1}{d}\ell_a(\mathbf{r}-\mathbf{r}')\right]g_{dd}^{aa}(\mathbf{r}-\mathbf{r}'). \qquad (64)
\end{aligned}
$$

C. Single-particle excitation spectrum

The single-particle potential of nuclear matter is calculated by applying the method devised in Ref. [28] to PB-FHNC theory and $N \neq Z$ matter. This will allow us to evaluate the single-particle neutron and proton potentials in neutron-rich matter.

TABLE IV. SNM energy per particle computed at $\rho = 0.016$ using the AT4′ potential. Our grid was set up to have 45 points in every direction.

d fm	1	3	3.1	3.2	3.3	3.35
E MeV	−0.73	−2.634	−2.787	−2.950	−3.087	−3.097

It is convenient to calculate, as in Ref. [28], the particle-hole excitation energy rather than directly the single-particle excitation, mainly because the $|\mathbf{ph}\rangle$ state has the same number of particles as the ground state. Let us consider,

$$
\epsilon_a(p,h) = \langle(\mathbf{p}_a\mathbf{h}_a\,|\,H\,|\,\mathbf{p}_a\mathbf{h}_a)\rangle_{\hat{p}_a,\hat{h}_a} - E_0, \qquad (65)
$$

where $(\mathbf{ph}\,|\,H\,|\,\mathbf{ph})$ is defined in Eq. (9), the label a specifies the isospin nature of the excitation, and $\langle\rangle$ stands for average over the directions of $\mathbf{p}$ and $\mathbf{h}$. As discussed in Sec. III A the variational estimates of diagonal states are maintained after orthogonalization. The single-particle excitation $\epsilon_a(q)$ can be obtained from $\epsilon_a(q,k_F) = \pm\epsilon_a(q) \mp \epsilon_{Fa}$, where the upper sign is for particle state ($q > k_F$) and the lower one for hole states ($q < k_F$), and

$$
\begin{aligned}
\epsilon_{Fa} &= \frac{E_0}{A} + \frac{\rho_a}{A}\frac{\partial E_0}{\partial\rho}, \\
&= \epsilon_0 + \rho_a\frac{\partial\epsilon_0}{\partial\rho}. \qquad (66)
\end{aligned}
$$

The single-particle spectrum is related to the real part of the nuclear optical potential by

$$
\epsilon_a(q) = \frac{\hbar^2 q^2}{2m} + U_a(q). \qquad (67)
$$

One can eliminate q from $\epsilon_a(q)$ and $U_a(q)$ to obtain an energy-dependent $U_a(\epsilon)$. Perturbative corrections to $\epsilon_a(q)$ and $U_a(q)$ include coupling with two-particle one-hole states $|\mathbf{p}',\mathbf{p}'',\mathbf{h}\rangle$ for $q > k_F$ or two-hole one-particle states $|\mathbf{h}',\mathbf{h}'',\mathbf{p}\rangle$, for $q < k_F$, giving a width to $|\mathbf{q}\rangle$.

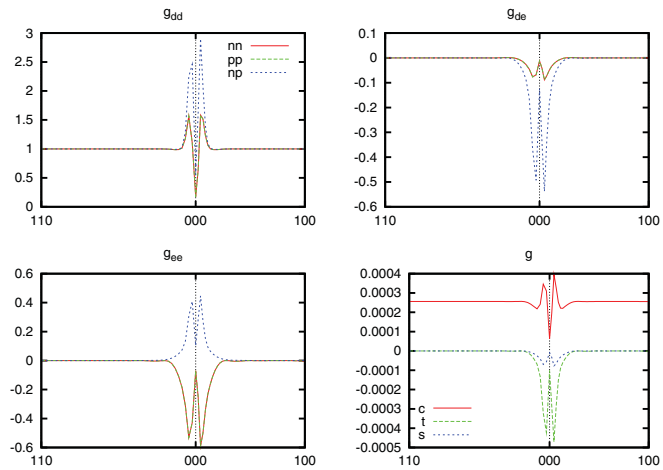

FIG. 9. (Color online) AT4′ g functions at $\rho = 0.016$ for $d = 3.30$.

TABLE V. Number of protons and neutrons for different admixtures that we studied and results at different densities.

Z	N	A	ΔA	%	α^2	$E(10^{-2}\rho_0)$	$E(10^{-1}\rho_0)$	$E(\rho_0)$	$E(\rho=0.25)$
0	1898	1898	0	0.00%	1.000	1.26	4.94	25.55	57.13
54	1850	1904	6	2.84%	0.890	1.16	4.28	20.78	47.52
114	1790	1904	6	5.99%	0.775	1.05	3.62	15.95	39.30
186	1694	1880	−18	9.89%	0.643	0.93	2.86	10.44	29.00
294	1598	1892	−6	15.54%	0.475	0.78	1.91	3.44	15.84
406	1502	1908	10	21.28%	0.330	0.65	1.08	−2.64	4.40
514	1382	1896	−2	27.11%	0.210	0.55	0.42	−7.55	−4.88
730	1174	1904	6	38.34%	0.054	0.42	−0.43	−13.84	−16.79
874	1030	1904	6	45.90%	0.007	0.38	−0.70	−15.88	−20.67

The particle-hole state $|\mathbf{p}_a\mathbf{h}_a)$ is generated in PB-FHNC theory by introducing the following density matrices:

$$l_a(\mathbf{r}_{ij};q_a;k_{Fa}) = l_a(\mathbf{r}_{ij}) + \Delta^a(\mathbf{r}_{ij};q_a;k_{Fa}),$$
$$\Delta^a(\mathbf{r}_{ij};q_a;k_{Fa}) = \pm\frac{1}{N_{\mathbf{q}_a}}\sum_{n\in\mathbf{q}_a}^{N_{\mathbf{q}_a}}\phi_n^*(i)\phi_n(j) \mp \frac{1}{N_{\mathbf{k}_{Fa}}}\sum_{n\in\mathbf{k}_{Fa}}^{\mathbf{k}_{Fa}}\phi_n^*(i)\phi_n(j), \quad (68)$$

where the summations are extended to the $N_{\mathbf{q}_a}$ states of the shell $\hbar^2q_a^2/(2m)$ and the $N_{\mathbf{k}_{Fa}}$ states of the shell $\hbar^2k_{Fa}^2/(2m)$.

The cluster diagrams contributing to $\epsilon_a(q,h)$ can be obtained by substituting in all the allowed diagrams of E_0 one and only one l_a line with a Δ^a line, for all the l_a lines of the diagram. To sum up the resulting series of cluster terms one can use the following algorithm:

(i) Modify the density matrices in the following way:

$$l_a \to l_a + x\Delta^a, \quad (69)$$

where x is a smallness parameter and serves to take only one Δ line at a time in each diagram.

(ii) Solve the PB-FHNC equations with the modified density matrices.

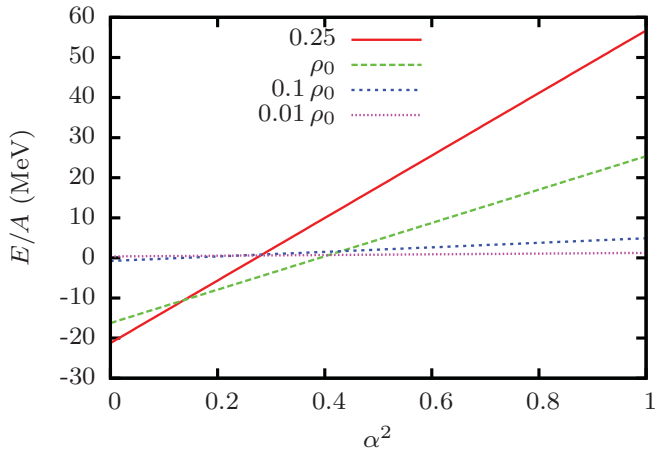

FIG. 10. (Color online) Energies per particle (E/A) of admixtures with different α^2 at different densities.

(iii) Compute the energy expectation value $\epsilon_a(\rho_N,\rho_P;q;k_F;x)$, as for the ground-state energy, with the Fermi energy given by

$$\epsilon_{Fa}(q,k_F) = \frac{\hbar^2}{2m}\left(\pm q^2 \mp k_{Fa}^2\right). \quad (70)$$

(iv) Compute the particle-hole excitation from

$$\epsilon_a(q,k_F) = \frac{\partial}{\partial x}\epsilon_a(\rho_N,\rho_P;q;k_F;x)|_{x=0}. \quad (71)$$

Note that the discrete character of PB-FHNC implies that ϵ_{Fa} will lie in between two energy shells, that we denote as ϵ_{Fa-} and ϵ_{Fa+}. It follows that the particle energies will be extracted from $\epsilon_a(p_a,k_{Fa-})$ and the hole states from $\epsilon_a(h_a,k_{Fa+})$. Therefore, one also needs to compute $\epsilon_a(k_{Fa+},k_{Fa-})$.

The neutron and proton effective masses are given by the derivatives,

$$\frac{m_a^*(\epsilon)}{m} = 1 = \frac{\partial U_a(\epsilon)}{\partial\epsilon}. \quad (72)$$

Enhancements of $m_a^*(\epsilon)$ will correspond to flattening of $U_a(\epsilon)$ around $\epsilon\sim\epsilon_{Fa}$ which, most likely, will happen only after having added the perturbative corrections [29].

VII. RESULTS

In this section we present and discuss *vertex corrected* PB-FHNC calculations, performed with the $\hat{F}_{JL}$ model, under the parallel-antiparallel approximation of Eq. (13) for the $AT4'$ and $(AV8')_4$ potentials.

We encoded our PB-FHNC scheme as an extension of the code already used in Ref. [19] and we refer the reader to that paper for details of the numerical techniques used. Whenever possible, we made use of standard libraries (e.g., fftw3) and routines documented elsewhere (e.g., the ODE integration

TABLE VI. Symmetry energy computed at different densities using the AT4′ potential.

ρ (fm^{-3})	$10^{-2}\rho_0$	$10^{-1}\rho_0$	ρ_0	0.25
S (MeV)	0.89	5.66	41.62	77.96

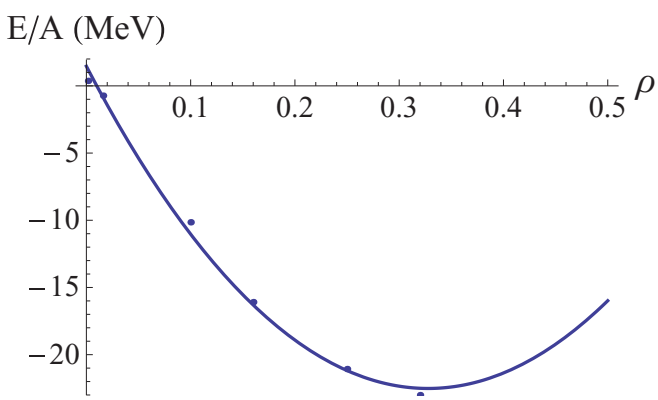

FIG. 11. (Color online) Energy per particle of SNM computed at different densities using the AT4′ potential. For low densities we forced the system to be homogeneous.

routines from Ref. [30]). We tested our double-precision code with different compilers and different optimizations, always obtaining consistent results.

A. Comparison of various correlated models

We tested our vertex corrected PB-FHNC scheme by comparing the results for SNM with the simple Jastrow ansatz with those of Ref. [19]. The results obtained for the expectation values of the kinetic energy, KE, the potential energy, PE, and the total energy, E, and displayed in the first and the fifth row of Table I coincide within five digits with those of Ref. [19]. Note that this check is not at all trivial because it follows from the fulfillment of the sum rule $\xi_d = 1$ and of the relations $\xi_e g_{de} = g^F_{de}$ and $\xi_e^2 g_{ee} = g^F_{ee}$, where g^F_{de} and g^F_{ee} are the *not vertex corrected* PB-FHNC distribution functions of Ref. [19].

We have analyzed the quality of our proposed variational model $\hat{F}_{JL}$ by comparing it against the results obtained with the $\hat{F}_2$ and $\hat{F}_4$ models for SNM at ρ_0. As shown in Table I, the longitudinal isospin-dependent model correlation $\hat{F}_{JL}$ improves considerably the Jastrow ansatz for the $AT4'$ potential. In addition, it gives equally good energy results as those of the $\hat{F}_2$ model. The effectiveness of $\tau_z(1)\tau_z(2)$ correlations as compared with the $\tau_1 \cdot \tau_2$ ones is confirmed by the results obtained with the $(AV8')_4$ potential which has a stronger $\sigma \cdot \sigma$ dependence. In Fig. 7, we show our correlation functions computed at $\rho = 0.16$. As expected from the Pauli exclusion principle, at $r = 0$ there is a stronger antiparallel correlation and weaker parallel one.

Tables II and III show the dependence of the energy results on the number of nucleons in the periodic box. One can see that with $A = 132$ finite size effects are still large. They become totally negligible at $A = 2060$ (see also Ref. [19])

B. Clustering at subnuclear densities

Although our variational ansatz does not allow an explicit clustering of the nucleonic matter, there are strong indications for such clustering phenomena for density below $0.1\rho_0$. To analyze these indications we have studied the behavior of total energy and of the pair distribution functions of SNM at $\rho = 0.1\rho_0$ in two different regions of the healing distance d. At small d ($d \sim 1$ fm) the correlation functions $f_\parallel$ and $f_\perp$ are below 1 for $r \leqslant d$, and the system does not show any clustering phenomena. On the contrary, as shown in Fig. 8, at large d ($3\,\text{fm} \leqslant d \leqslant 3.35\,\text{fm}$) the correlation functions have pronounced peaks, occurring roughly at the same value of the interparticle distance, irrespective of the value of d, as typically happens in clustering phenomena. One can see from Table IV that the variational energy gets lower in the region of large d reaching a minimum around $d \sim 3.3$ fm.

In Table IV we show the energy of a system of 2060 nucleons (SNM) computed with different healing distances. For all these calculations we enforced the same level of convergence of our FHNC equations. For $d > 3.35$ fm we were not able to make our equations converge any longer. For comparison we show the energy obtained with $d = 1$ fm which is the largest healing length that does not produce the clustering effect.

In Fig. 9 we show our results, obtained with $d = 3.30$ fm for the various g components and for g_{dd}, g_{de}, and g_{ee}. It is easy to see that indeed in the channel np there is a clear evidence of clustering occurring.

Our results strongly indicate that at such low densities variational functions allowing for a nucleus embedded in a neutron fluid would have a lower energy with respect to those describing an homogeneous fluid. In the following we have always forced the system to behave as an homogeneous fluid.

C. Symmetry energy at subnuclear densities

One of the main advantages of a $\tau_{z1}\tau_{z2}$ form of the isospin correlations is that one can easily compute the energy expectation value of nuclear matter with $N \neq Z$, provided that both N and Z are magic numbers (i.e., they correspond to shell closure). For this reason, we cannot keep $A = N + Z$ fixed. The average value of A which we find more convenient because it is sufficiently large to reduce finite size effects and allows for a quite large number of admixtures with the smallest fluctuations (ΔA) is the magic number 1898. In Table V we report the number of protons and neutrons for each admixture, the percentage $Z/A = 0.5(1 - \alpha)$, and the energy results of our calculations—performed using AT4′ potential—at four different densities.

We used our results to check whether the standard way of fitting asymmetric admixture energies (i.e., using a simple quadratic fit) can be reliably used at subnuclear densities. We used MATHEMATICA to fit our results using a sixth-degree polynomial as a prior. As expected we get null coefficients for the odd power terms. We also get nonzero coefficients for the fourth power term. Such coefficients, however, are always negligible, being at most one order of magnitude smaller than the second power term one.

In Fig. 10 we show our results and our fits for the energies (E) of admixtures with different α^2. In Table VI we give our best estimate for the symmetry energy (S) at different densities computed using the AT4′ potential and a purely quadratic fit. The value obtained at ρ_0 is somewhat larger

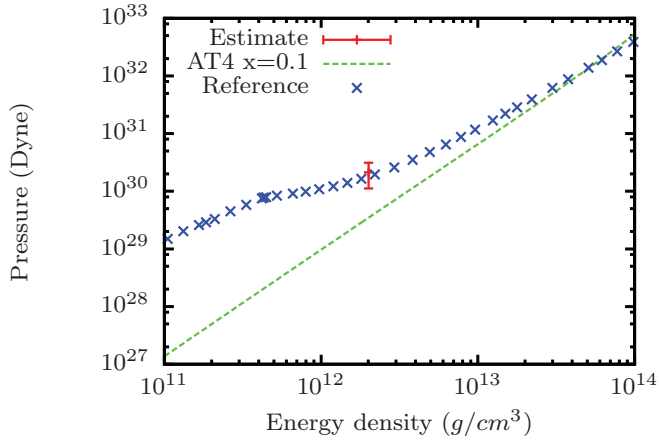

FIG. 12. (Color online) Equation of state for matter at subnuclear densities; see text for details.

than the experimental results of $S \sim 36$ MeV; this is expected because of the phenomenological nature of our potential.

D. Equations of state for AT4′

In Fig. 11 we show our results for the energy of SNM computed at different densities using the AT4′ potential. We find that we can nicely fit our data by

$$E_{\rm SNM}(\rho) = E_0 + a(\rho - \rho_{\rm eq})^2 + b(\rho - \rho_{\rm eq})^3 e^{\gamma(\rho - \rho_{\rm eq})}, \quad (73)$$

where $E_0 = -22.51$ MeV, $\rho_{\rm eq} = 0.33\,{\rm fm}^{-3}$, $a = 220\,{\rm MeV\,fm}^6$, $b = -1.56\,{\rm MeV\,fm}^9$, and $\gamma = -5.570\,{\rm fm}^3$. The EOS for asymmetric matter can then be written, fitting the data for different α, as

$$E(\rho, \alpha) = E_{\rm SNM}(\rho) + C_s \left(\frac{\rho}{\rho_{\rm eq}}\right)^{\gamma_s} \alpha^2, \quad (74)$$

where $C_s = 82.86$ MeV and $\gamma_s = 0.913$.

In Fig. 12 we show our EOS at subnuclear density computed in two cases: PNM and 10% protons. We show in the same plot the BPS EOS [31] as a useful comparison. Quite comfortingly our results show quite a good agreement at the edge of the inner crust. This agreement is obviously not preserved at lower densities because of the absence of clusters. In the same diagram we also show a point computed subtracting, from the energy of the pure gas, the binding energy of the corresponding nucleus (as reported by Ref. [32]) obtained using the semiempirical mass formula. We used different polynomials to fit $E(\rho)$ and hence to derive P. The error bars show our best estimate obtained using a cubic spline interpolation.

E. Particle hole

In Fig. 13 we show our results for the single-particle energy in different test cases as a function of $q = p - k_f$. The values at $q = 0$ are given by the corresponding chemical potentials ϵ_{Fa} given in Eq. (66). The correlation effects can be viewed by comparing the $\hat{F}_4$ results with the corresponding Fermi gas estimates. Our results at ρ_0 and $\alpha = 0$ are in reasonably good agreement with the FHNC/SOC calculations of Ref. [29] obtained with the Urbana V_{14} + TNR interaction. One can see that at lower densities the effects on the optical potential from the asymmetry are much reduced.

VIII. CONCLUSIONS AND PERSPECTIVES

We have made a first step toward the development of a technique, based on CBF theory, allowing for a study of the NS crust from first principles. In particular we have developed a theoretical framework suitable for studying NS crustal cells using v_4 potentials and we have applied it, using the AT4′ potential as a test case.

Our results are promising in several respects. First of all it is shown that using only the third component of the isospin dependent correlation is a good enough approximation. We are in a good position, from the variational point of view, to insert a nucleus in our system as discussed in the introduction. We are also in a good position to rewrite the FHNC/SOC scheme, and the CBF perturbative corrections, using this simplified operator to treat the isospin. This would enable us to use more realistic potentials (particularly those with tensor interaction) and hence to refine our results. Notice that standard FHNC/SOC does not allow for asymmetric matter.

Moreover the vertex corrected theory developed here can be readily used to include superfluid effects, thus improving the accuracy of our description of the crustal matter.

Finally the extension of PB-FHNC theory to the treatment of asymmetric matter is essential to deal with the crustal matter,

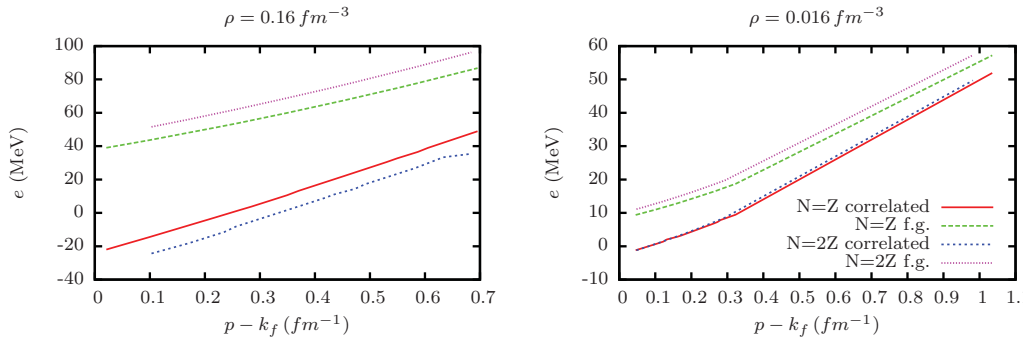

FIG. 13. (Color online) Single-particle energy $e(p)$ for $N = Z$ and $N = 2Z$ at $\rho = 0.16\,{\rm fm}^{-3}$ and $\rho = 0.016\,{\rm fm}^{-3}$ computed using the AT4′ potential. The figures report also the Fermi gas estimates.

thus, enabling a fully self-consistent description of the neutron star equation of state.

ACKNOWLEDGMENTS

This work was partially supported by CompStar, a Research Networking Programme of the European Science Foundation. This work was partially funded under the MIUR PRIN fund "Fermi Hypernetted Chain and Quantum Monte Carlo Studies of Nuclei and Nuclear Matter with Applications to the Astrophysics of Neutron Stars," and National Science Foundation (Grant No. PHY0757703).

APPENDIX A: COMPUTATION OF CORRELATIONS

To compute the correlation function needed for our calculation, we have to solve a set of differential equations which can be derived by minimizing the expectation value of the energy given by the lowest order diagrams, as shown in Ref. [26]. The expectation value of the energy is

$$E_{LO} = \frac{1}{2\rho}\int_\Omega d\mathbf{r}\left\{\frac{\hbar^2}{m}(\nabla f_\parallel)^2\left[\rho_N^2\left(1-\frac{1}{2}\ell_N^2\right)+\rho_P^2\left(1-\frac{1}{2}\ell_P^2\right)\right]+f_\parallel^2\left[(\upsilon_c+\upsilon_\tau)\left(\rho_N^2\left(1-\frac{1}{2}\ell_N^2\right)+\rho_P^2\left(1-\frac{1}{2}\ell_P^2\right)\right)\right.\right.$$
$$\left.\left.-3\,(\upsilon_\sigma+\upsilon_{\sigma\tau})\left(\frac{1}{2}\rho_P^2\ell_P^2+\frac{1}{2}\rho_N^2\ell_N^2\right)\right]\right\}+\frac{\rho_P\rho_N}{\rho}\int_\Omega d\mathbf{r}\left\{\frac{\hbar^2}{m}(\nabla f_\perp)^2+f_\perp^2\left[(\upsilon_c-\upsilon_\tau)-4\frac{\ell_P}{2}\frac{\ell_N}{2}(\upsilon_\tau+3\upsilon_{\sigma\tau})\right]\right\}. \tag{A1}$$

Minimizing this expression with respect to $f_\parallel$ and $f_\perp$ gives

$$\begin{aligned}&-\frac{\hbar^2}{m}(\nabla f_\perp)^2+f_\perp[\upsilon_c-\upsilon_\tau-\ell_P\ell_n N(\upsilon_\tau+3\upsilon_{\sigma\tau})]=0,\\&-\frac{\hbar^2}{m}[(\nabla f_\parallel)^2G+\nabla f_\parallel(\nabla G)]+f_\parallel\big[(\upsilon_c+\upsilon_\tau)G\\&\quad-3(\upsilon_\sigma+\upsilon_{\sigma\tau})\big(\rho_N^2+\rho_P^2-G\big)\big]=0,\end{aligned} \tag{A2}$$

where

$$G=\rho_N^2\left(1-\tfrac{1}{2}\ell_N^2\right)+\rho_P^2\left(1-\tfrac{1}{2}\ell_P^2\right). \tag{A3}$$

Without any loss of generality, we can divide each term of the second equation by ρ^2 and redefine G accordingly. In the following, we set $\zeta_a=\rho_a/\rho$.

These two differential equations need to be solved bearing in mind that f should heal smoothly to one at some distance d. For easily solving them, it is convenient to start from $r=0$ after having redefined the variables:

$$\phi_\perp=rf_\perp,\quad \psi_\parallel=r\sqrt{G}f,$$

with

$$\begin{aligned}&\phi_\perp(d)=d\quad \phi'_\perp(d)=1,\\&\psi_\parallel(d)=d\sqrt{G(d)}\quad \psi'_\parallel(d)=\sqrt{G(d)}+\frac{1}{2}\frac{dG'(d)}{\sqrt{G(d)}}.\end{aligned}$$

These two new functions are defined so that their value at the origin is zero. Since there are then three boundary conditions, we need to introduce two lagrange multipliers λ to ensure that they are all satisfied simultaneously. This leads to

$$\begin{aligned}&-\frac{\hbar^2}{m}\phi''_\perp+\phi_\perp[\upsilon_c-\upsilon_\tau-\ell_p\ell_n(\upsilon_\tau+3\upsilon_{\sigma\tau})]=\lambda_\phi\phi_\perp,\\&-\frac{\hbar^2}{m}\psi''_\parallel+\psi_\parallel\left[\frac{(\upsilon_c+\upsilon_\tau)G-3(\upsilon_\sigma+\upsilon_{\sigma\tau})\big(\zeta_n^2+\zeta_p^2-G\big)}{G}\right.\\&\quad\left.+\frac{\hbar^2}{m}\left(\frac{1}{2}\frac{G''}{G}+\frac{G'}{rG}-\frac{1}{4}\frac{G'^2}{G^2}\right)\right]=\lambda_\psi\psi_\parallel.\end{aligned} \tag{A4}$$

We solve these two equations using a standard adaptive-stepsize Bulirsch-Stoer method, varying d so as to minimize the energy and iterating to evaluate the λs. The equations have the form,

$$\phi''+(a(r)-\lambda)\phi=0, \tag{A5}$$

and we can adjust λ by adding, at each iteration, a $\delta\lambda$ defined as

$$\delta\lambda=\frac{\phi_T(d)\phi'_C(d)-\phi_C(d)\phi'_T(d)}{\int_0^d\phi_C^2}, \tag{A6}$$

where the quantities denoted with a subscript C are those computed numerically at the previous step, and those with a subscript T are theoretically derived boundary conditions which need to be satisfied at $r=d$.

APPENDIX B: SOME STANDARD QUANTUM MECHANICS RESULTS

As a useful reference we recall that

$$\mathcal{A}[\psi_1^*\cdots\psi_N^*]\hat{O}(x_1,\ldots,x_n)\mathcal{A}[\psi_1\cdots\psi_N] \tag{B1}$$

can be rewritten as

$$\frac{1}{\sqrt{N!}}\sum_{i=1,i\neq j}^{N}[\psi_1^*\cdots\psi_N^*]\hat{O}(x_1,\ldots,x_n)\mathcal{A}[\psi_1\ldots\psi_N]. \tag{B2}$$

The antisymmetrizing operator can be written in terms of the two-particle exchange operator P:

$$\begin{aligned}\mathcal{A}=1-\sum_{i<j}P_{ij}+\sum_{i<j<k}(P_{ij}P_{jk}+P_{ik}P_{kj})\\+\sum_{i<j<k<l}(P_{ij}P_{kl}+P_{ik}P_{jl}+P_{il}P_{jk})\\-\{ijkl\text{ loop}\}+\cdots.\end{aligned} \tag{B3}$$

Applying Eq. (B3), it is easy to check that the Fermi gas n-body correlation function is given by

$$g_n^{FG}(\mathbf{r}_1,\ldots,\mathbf{r}_n) = 1 - \sum_{a,(i<j)} \frac{1}{d}\ell_a(\mathbf{r}_{i,j})^2 + \sum_{a,(i<j<k)} \frac{2}{d^3}\ell_a(\mathbf{r}_{i,j})\ell_a(\mathbf{r}_{j,k})\ell_a(\mathbf{r}_{k,i}) + \cdots . \tag{B4}$$

and, in a more compact form, by the following determinant:

$$g_n^{FG}(\mathbf{r}_1,\ldots,\mathbf{r}_n) = \begin{vmatrix} 1 & \frac{1}{d}\sum_a \ell_a(1,2) & \frac{1}{d}\sum_a \ell_a(1,3) & \ldots & \frac{1}{d}\sum_a \ell_a(1,n) \\ \frac{1}{d}\sum_a \ell_a(2,1) & 1 & \frac{1}{d}\sum_a \ell_a(2,3) & \ldots & \frac{1}{d}\sum_a \ell_a(2,n) \\ \ldots & \ldots & \ldots & \ldots & \ldots \\ \frac{1}{d}\sum_a \ell_a(n,1) & \frac{1}{d}\sum_a \ell_a(A,2) & \frac{1}{d}\sum_a \ell_a(n,3) & \ldots & 1 \end{vmatrix},$$

where $\ell_a(i,j)$ and $\ell_a(\mathbf{r}_{i,j})$ are defined in Eq. (16), the summations run over the isospin states, $(a = N, P)$, and $d = 2$. The products of the $\ell_a(i,j)$ operators also imply the matrix elements of the relative spin-isospin states (all the spin-isospin states of the particle in a loop must be the same). In infinite matter $\ell_a(\mathbf{r}_{i,j})$ reduces to

$$\ell_a(\mathbf{r}_{i,j}) = \ell(x = k_{Fa}r_{ij}) = \frac{3}{x^3}[\sin(x) - x\cos(x)]. \tag{B5}$$

[1] C. M. Espinoza, A. G. Lyne, B. W. Stappers, and M. Kramer, Mon. Not. R. Astron. Soc. **414**, 1679 (2011).
[2] N. Chamel and P. Haensel, Living Rev. Relativity **11**, 10 (2008) [http://www.livingreviews.org/lrr-2008-10].
[3] A. Pastore, F. Barranco, R. A. Broglia, and E. Vigezzi, Phys. Rev. C **78**, 024315 (2008).
[4] H. S. Than, E. Khan, and N. Van Giai, J. Phys. G **38**, 025201 (2010).
[5] G. G. Raffelt, *The Stars as Laboratories of Fundamental Physics* (University of Chicago, Chicago, 1996).
[6] E. Feenberg, *Theory of Quantum Fluids* (Academic Press, New York, 1969).
[7] J. W. Clark, L. R. Mead, E. Krotscheck, K. E. Kurten, and L. Ristig, Nucl. Phys. A **328**, 45 (1979).
[8] E. Krotscheck and J. W. Clark, Nucl. Phys. A **328**, 73 (1979).
[9] S. Fantoni and V. R. Pandharipande, Phys. Rev. C **37**, 1697 (1988).
[10] K. E. Schmidt and S. Fantoni, Phys. Lett. B **446**, 99 (1999).
[11] L. Engvik, M. Hjorth-Jensen, E. Osnes, G. Bao, and E. Østgaard, Phys. Rev. Lett. **73**, 2650 (1994).
[12] R. B. Wiringa, V. G. J. Stoks, and R. Schiavilla, Phys. Rev. C **51**, 38 (1995).
[13] J. Carlson, V. R. Pandharipande, and R. B. Wiringa, Nucl. Phys. A **401**, 59 (1983).
[14] A. Lovato, O. Benhar, S. Fantoni, A. Y. Illarionov, and K. E. Schmidt, Phys. Rev. C **83**, 054003 (2011).
[15] I. E. Lagaris and V. R. Pandharipande, Nucl. Phys. A **359**, 331 (1981).
[16] B. S. Pudliner, V. R. Pandharipande, J. Carlson, S. C. Pieper, and R. B. Wiringa, Phys. Rev. C **56**, 1720 (1997).
[17] R. B. Wiringa and S. C. Pieper, Phys. Rev. Lett. **89**, 182501 (2002).
[18] I. R. Afnan and Y. C. Tang, Phys. Rev. **175**, 1337 (1968).
[19] S. Fantoni and K. E. Schmidt, Nucl. Phys. A **690**, 456 (2001).
[20] V. R. Pandharipande and R. B. Wiringa, Rev. Mod. Phys. **51**, 821 (1979).
[21] S. Fantoni and S. Rosati, Il Nuovo Cimento A **25**, 593 (1975).
[22] S. Fantoni and A. Fabrocini, in *Lecture Notes in Physics*, Vol. 510, edited by J. Navarro and A. Polls (Springer-Verlag, Berlin, 1998), pp. 119–186.
[23] S. Fantoni, A. Sarsa, and K. E. Schmidt, Phys. Rev. Lett. **87**, 181101 (2001).
[24] A. Münster, *Statistical Thermodynamics* (Academic Press, New York, 1970).
[25] A. Fabrocini, S. Fantoni, S. Rosati, and A. Polls, Phys. Rev. B **33**, 6057 (1986).
[26] R. B. Wiringa, V. Fiks, and A. Fabrocini, Phys. Rev. C **38**, 1010 (1988).
[27] S. Fantoni and S. Rosati, Phys. Lett. B **84**, 23 (1979).
[28] B. Friedman and V. Pandharipande, Phys. Lett. B **100**, 205 (1981).
[29] S. Fantoni, B. L. Friman, and V. R. Pandharipande, Nucl. Phys. A **399**, 51 (1983).
[30] W. H. Press and N. R. S. Firm, *Numerical Recipes in FORTRAN 77 and FORTRAN 90: The Art of Scientific and Parallel Computing* (Cambridge University Press, New York, 1996).
[31] G. Baym, C. Pethick, and P. Sutherland, Astrophys. J. **170**, 299 (1971).
[32] J. W. Negele and D. Vautherin, Nucl. Phys. A **207**, 298 (1973).